Table 3
Immunoblot assay of ganglioside GM1 amount.

	4 weeks	8 weeks	6 months
Age-matched non-treated (range)	2.65–3.55 ($n = 3$)	4.98–5.28 ($n = 3$)	7.58 (n = 1)
Treated with uncultured FBC	Mouse I	Mouse VI	Mouse XI
	Rt: 1.42[a]	Rt: 2.30[a]	Rt: 6.18[b]
	Lt: 1.80[a]	Lt: 2.44[a]	Lt: 6.40[b]
Treated with MSC	Mouse II	Mouse VII	
	Rt: 1.82[a]	Rt: 5.30	
	Lt: 1.31[a]	Lt: 5.23	
	Mouse III	Mouse VIII	
	Rt: 1.40[a]	Rt: 4.40[b]	
	Lt: 1.34[a]	Lt: 4.73[b]	
Treated with mixed MSC and FBC	Mouse IV	Mouse IX	
	Rt: 1.33[a]	Rt: 4.55[b]	
	Lt: 1.34[a]	Lt: 4.78[b]	
	Mouse V	Mouse X	
	Rt: 1.78[a]	Rt: 4.45[b]	
	Lt: 1.62[a]	Lt: 4.58[b]	

Values are ratios to those for age-matched control mice. Each sample was tested in duplicate for three times and results are mean values. Rt, right hemisphere; Lt, left hemisphere.

[a] Remarkable decrease.
[b] Slight decrease of ganglioside GM1 compared with non-treated mice.

was found in the mice of every group. However, at 8 weeks, decrease was detected only in the mouse treated with FBC. Efficacy was still noted at 6 months after injection in FBC-treated mouse. These findings were consistent with those for X-Gal staining (Fig. 1) and β-galactosidase activity (Table 2).

4. Discussion

Two therapeutic methods, HSCT and ERT, are clinically available for LSDs. However, neither is markedly effective in the brain. A number of experiments in animal models have been carried out on the treatment of brain in LSDs. Each revealed some efficacy in the brain, though it was transient and incomplete. Sufficient enzyme expression throughout life is needed in the brain. Thus, permanent engraftment of enzyme-secreting cells in the brain, or permanent expression of an exogenous gene with a vector or as an integrated gene might eliminate the brain involvement in LSDs.

However, the immune responses of host animals are among the most difficult problems to overcome in this respect [31–33]. Although the brain, which is sequestered from systemic immune responses, is thought to exhibit little immune response, elimination of cells expressing a therapeutic transgene occurs in the brain. We speculate that innate inflammatory immune responses are stimulated to kill such cells, not necessarily with the induction of a linked adaptive immune response. When host brain cells express a therapeutic transgene mediated by a viral vector, the host cells themselves will be eliminated, possibly resulting in acceleration of neuronal cell death in neurodegenerative disorders. Transplantation of cells having the same genetic information as the host

animals with LSD except for expression of a deficient enzyme protein would thus be a good method of treatment for avoiding the elimination of host neuronal cells and curing diseased host cells.

We performed cell transplantation into the brain of β-galactosidase-deficient mice to study the usefulness of long-term engraftment for supplementation of deficient enzyme protein. To minimize the immune responses in the recipient β-galactosidase knock-out mice, we used cells of mice with the same genetic background as the recipient except for possession of copies of the human β-galactosidase gene.

Initially, in the transplantation experiment, we used FBC from transgenic mice expressing the human β-galactosidase gene. The cells could grow in an environment similar to that of the recipient organ in which they were originally growing. The cells spread into the brains and the cell number increased at least until 4 weeks. They grew very successfully for at least 8 weeks and survived for 6 months or more. However, the number of engrafted cells had decreased significantly at 6 months, while the size of the brain had increased. The decrease in ganglioside GM1 accumulation was also marked until 8 weeks after transplantation. However, at 6 months, this decrease was far less pronounced, with re-accumulation of ganglioside GM1. After the cells were engrafted and the cell number was increased by the cell division in the recipient brain, they were depleted. The mechanism of depletion of transplanted cells involved immunological rejection, although the transplanted cells were very similar genetically and physiologically to the recipient.

Next, we performed a transplantation experiment using MSCs obtained from the bone marrow of the

Wild-type mouse   a

Non-treated mouse   b

FBC-treated mouse
Right hemisphere   c

FBC-treated mouse
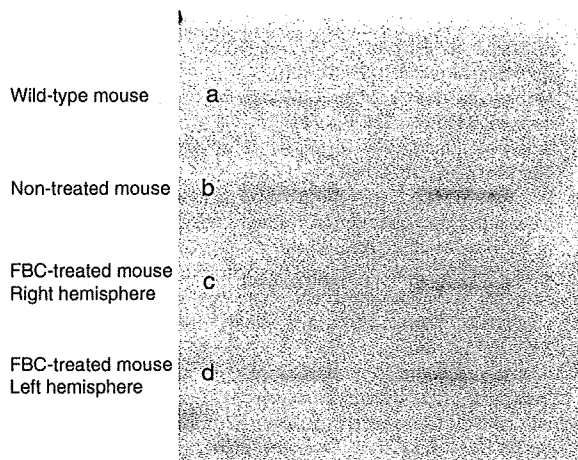Left hemisphere   d

Fig. 2. Immunoblot assay of ganglioside GM1 in brain homogenate at 8 weeks after treatment. Performed in duplicate as shown in two slots for each sample. (a) Wild-type mouse; (b) Non-treated mouse; (c and d) Right and left hemisphere, respectively, of a mouse treated with FBC. The immunoreactivity against ganglioside GM1 antibody in the treated brain (c and d) was less than non-treated brain (d). The accumulated amounts of ganglioside GM1 were calculated in the ratio to the age-matched wild-type mouse (a) from the densitometric quantification signals. These values were shown in Table 3.

same mice expressing the human β-galactosidase gene. MSCs were obtained using the method of plastic adherence. This relatively crude procedure produces a heterogeneous population including multipotential MSCs. These crude cells were used to avoid depletion of potentially important cells and for ease of preparation for clinical application. The cells spread into the brains and the cell number increased similarly to FBC transplantation experiment until 4 weeks. However, decrease in number of engrafted living cells and efficacy in preventing accumulation of ganglioside GM1 were observed in the examination of 8-week-old treated mice.

A number of studies on neural transdifferentiation have been reported [34–37]. Some have reported that neural transdifferentiation of MSCs is induced by cell fusion with host neuronal cells [38–41]. We therefore used mixed FBC and MSC cells to stimulate cell fusion. More engrafted cells were found in the deep areas of the mouse brains treated with mixed cells than in the brains treated with MSC alone. However, no fused cells could be identified. The long-living cells were probably transplanted FBC themselves.

Decrease of ganglioside GM1 was observed even though the increase of the β-galactosidase activity was so small. Similar efficacy was shown previously in our gene therapy experiment [2]. On the other hand, we observed a general depletion of the transplanted cells over time in the BKO mouse brains. The transplanted cells survived in early stage and the number increased by cell division, then, died. This was likely caused by immunological rejection, even though we used fetal brain cells (FBC) from mice with the same genetic background for transplantation. We speculated that immunological reaction occurred because these cells expressed the therapeutic enzyme protein which the host animals did not have. The same has been reported in the transplantation of autogenous cells expressing an exogenous therapeutic gene [33]. The grafted cells were gradually depleted because of immunological rejection by the host animals. To avoid deleterious immune attack and to achieve sufficient long-term efficacy in brain, development of methods to steer the immune response away from cytotoxic responses or to induce tolerance to the products of therapeutic genes is needed [42,43].

References

[1] Shen JS, Watabe K, Ohashi T, Eto Y. Intraventricular administration of recombinant adenovirus to neonatal twitcher mouse leads to clinicopathological improvements. Gene Ther 2001;8:1081–7.

[2] Takaura N, Yagi T, Maeda M, Nanba E, Oshima A, Suzuki Y, et al. Attenuation of ganglioside GM1 accumulation in the brain of GM1 gangliosidosis mice by neonatal intravenous gene transfer. Gene Ther 2003;10:1487–93.

[3] Kim EY, Hong YB, Lai Z, Cho YH, Brady RO, Jung SC. Long-term expression of the human glucocerebrosidase gene in vivo after transplantation of bone-marrow-derived cells transformed with a lentivirus vector. J Gene Med 2005;7:878–87.

[4] Shen JS, Meng XL, Yokoo T, Sakurai K, Watabe K, Ohashi T, et al. Widespread and highly persistent gene transfer to the CNS by retrovirus vector in utero: implication for gene therapy to Krabbe disease. J Gene Med 2005;7:540–51.

[5] Cachón-González MB, Wang SZ, Lynch A, Ziegler R, Cheng SH, Cox TM. Effective gene therapy in an authentic model of Tay-Sachs-related diseases. Proc Natl Acad Sci USA 2006;103:10373–8.

[6] Kopen GC, Prockop DJ, Phinney DG. Marrow stromal cells migrate throughout forebrain and cerebellum, and they differentiate into astrocytes after injection into neonatal mouse brains. Proc Natl Acad Sci USA 1999;96:10711–6.

[7] Jin HK, Carter JE, Huntley GW, Schuchman EH. Intracerebral transplantation of mesenchymal stem cells into acid sphingomyelinase-deficient mice delays the onset of neurological abnormalities and extends their life span. J Clin Invest 2002;109:1183–91.

[8] Sakurai K, Iizuka S, Shen JS, Meng XL, Mori T, Umezawa A, et al. Brain transplantation of genetically modified bone marrow stromal cells corrects CNS pathology and cognitive function in MPS VII mice. Gene Ther 2004;11:1475–81.

[9] Givogri MI, Galbiati F, Fasano S, Amadio S, Perani L, Superchi D, et al. Oligodendroglial progenitor cell therapy limits central

neurological deficits in mice with metachromatic leukodystrophy. J Neurosci 2006;26:3109–19.

[10] Kakkis E, McEntee M, Vogler C, Le S, Levy B, Belichenko P, et al. Intrathecal enzyme replacement therapy reduces lysosomal storage in the brain and meninges of the canine model of MPS I. Mol Genet Metab 2004;83:163–74.

[11] Dickson P, McEntee M, Vogler C, Le S, Levy B, Peinovich M, et al. Intrathecal enzyme replacement therapy: successful treatment of brain disease via the cerebrospinal fluid. Mol Genet Metab 2007;91:61–8.

[12] Vogler C, Levy B, Grubb JH, Galvin N, Tan Y, Kakkis E, et al. Overcoming the blood–brain barrier with high-dose enzyme replacement therapy in murine mucopolysaccharidosis VII. Proc Natl Acad Sci USA 2005;102:14777–82.

[13] Matzner U, Herbst E, Hedayati KK, Lüllmann-Rauch R, Wessig C, Schröder S, et al. Enzyme replacement improves nervous system pathology and function in a mouse model for metachromatic leukodystrophy. Hum Mol Genet 2005;14:1139–52.

[14] Blanz J, Stroobants S, Lüllmann-Rauch R, Morelle W, Lüdemann M, D'Hooge R, et al. Reversal of peripheral and central neural storage and ataxia after recombinant enzyme replacement therapy in {alpha}-mannosidosis mice. Hum Mol Genet 2008;17:3437–45.

[15] Grubb JH, Vogler C, Levy B, Galvin N, Tan Y, Sly WS. Chemically modified {beta}-glucuronidase crosses blood–brain barrier and clears neuronal storage in murine mucopolysaccharidosis VII. Proc Natl Acad Sci USA 2008;105:2616–21.

[16] Montaño AM, Oikawa H, Tomatsu S, Nishioka T, Vogler C, Gutierrez MA, et al. Acidic amino acid tag enhances response to enzyme replacement in mucopolysaccharidosis type VII mice. Mol Genet Metab 2008;94:178–89.

[17] Kasperzyk JL, El-Abbadi MM, Hauser EC, D'Azzo A, Platt FM, Seyfried TN. N-butyldeoxygalactonojirimycin reduces neonatal brain ganglioside content in a mouse model of GM1 gangliosidosis. J Neurochem 2004;89:645–53.

[18] Lachmann RH, te Vruchte D, Lloyd-Evans E, Reinkensmeier G, Sillence DJ, Fernandez-Guillen L, et al. Treatment with miglustat reverses the lipid-trafficking defect in Niemann-Pick disease type C. Neurobiol Dis 2004;16:654–8.

[19] Cox TM. Substrate reduction therapy for lysosomal storage diseases. Acta Paediatr Suppl. 2005;94:69–75.

[20] Piotrowska E, Jakóbkiewicz-Banecka J, Barańska S, Tylki-Szymańska A, Czartoryska B, Wegrzyn A, et al. Genistein-mediated inhibition of glycosaminoglycan synthesis as a basis for gene expression-targeted isoflavone therapy for mucopolysaccharidoses. Eur J Hum Genet 2006;14:846–52.

[21] Ishii S, Yoshioka H, Mannen K, Kulkarni AB, Fan JQ. Transgenic mouse expressing human mutant alpha-galactosidase A in an endogenous enzyme deficient background: a biochemical animal model for studying active-site specific chaperone therapy for Fabry disease. Biochim Biophys Acta 2004;1690:250–7.

[22] Matsuda J, Suzuki O, Oshima A, Yamamoto Y, Noguchi A, Takimoto K, et al. Chemical chaperone therapy for brain pathology in G(M1)-gangliosidosis. Proc Natl Acad Sci USA 2003;100:15912–7.

[23] Matsuda J, Suzuki O, Oshima A, Ogura A, Noguchi Y, Yamamoto Y, et al. Beta-galactosidase-deficient mouse as an animal model for GM1-gangliosidosis. Glycoconj J 1997;14:729–36.

[24] Yamamoto Y, Nagase Y, Noguchi A, Mochida K, Nakahira M, Takano K, et al. Generation and characterization of the β-galactosidase knockout mouse having the normal human β-galactosidase gene as a transgene (in Japanese). Proc Jap Soc of Animal Models for Hum Dis (Nippon Shikkan Model Gakkai Kiroku) 2001;17:20–2.

[25] Meirelles Lda S, Nardi NB. Murine marrow-derived mesenchymal stem cell: isolation, in vitro expansion, and characterization. Br J Haematol 2003;123:702–11.

[26] Meberg PJ, Miller MW. Culturing hippocampal and cortical neurons. Methods Cell Biol 2003;71:111–27.

[27] Suzuki K. Enzymatic diagnosis of sphingolipidosis. Methods Enzymol 1987;138:727–62.

[28] Bradford MM. A Rapid and sensitive method for the quantitation of microgram quantities of protein utilizing the principle of protein-dye binding. Anal Biochem 1976;72:255–60.

[29] Michikawa M, Gong JS, Fan QW, Sawamura N, Yanagisawa K. A novel action of alzheimer's amyloid beta-protein (Abeta): oligomeric Abeta promotes lipid release. J Neurosci 2001;21:7226–35.

[30] Suzuki Y, Ichinomiya S, Kurosawa M, Ohkubo M, Watanabe H, Iwasaki H, et al. Chemical chaperone therapy: clinical effect in murine G(M1)-gangliosidosis. Ann Neurol 2007;62:671–5.

[31] Barker RA, Widner H. Immune problems in central nervous system cell therapy. NeuroRx 2004;1:472–81.

[32] Abordo-Adesida E, Follenzi A, Barcia C, Sciascia S, Castro MG, Naldini L, et al. Stability of lentiviral vector-mediated transgene expression in the brain in the presence of systemic antivector immune responses. Hum Gene Ther 2005;16:741–51.

[33] Lowenstein PR, Kroeger K, Castro MG. Immunology of neurological gene therapy: how T cells modulate viral vector-mediated therapeutic transgene expression through immunological synapses. Neurotherapeutics 2007;4:715–24.

[34] Weimann JM, Charlton CA, Brazelton TR, Hackman RC, Blau HM. Contribution of transplanted bone marrow cells to Purkinje neurons in human adult brains. Proc Natl Acad Sci USA 2003;100:2088–93.

[35] Abouelfetouh A, Kondoh T, Ehara K, Kohmura E. Morphological differentiation of bone marrow stromal cells into neuron-like cells after co-culture with hippocampal slice. Brain Res 2004;1029:114–9.

[36] Wislet-Gendebien S, Hans G, Leprince P, Rigo JM, Moonen G, Rogister B. Plasticity of cultured mesenchymal stem cells: switch from nestin-positive to excitable neuron-like phenotype. Stem cells 2005;23:392–402.

[37] Deng J, Petersen BE, Steindler DA, Jorgensen ML, Laywell ED. Mesenchymal stem cells spontaneously express neural proteins in culture and are neurogenic after transplantation. Stem cells 2006;24:105410–64.

[38] Terada N, Hamazaki T, Oka M, Hoki M, Mastalerz DM, Nakano Y, et al. Bone marrow cells adopt the phenotype of other cells by spontaneous cell fusion. Nature 2002;416:542–5.

[39] Alvarez-Dolado M, Pardal R, Garcia-Verdugo JM, Fike JR, Lee HO, Pfeffer K, et al. Fusion of bone-marrow-derived cells with Purkinje neurons, cardiomyocytes and hepatocytes. Nature 2003;425:968–73.

[40] Kozorovitskiy Y, Gould E. Stem cell fusion in the brain. Nat Cell Biol 2003;5:952–4.

[41] Bae JS, Furuya S, Shinoda Y, Endo S, Schuchman EH, Hirabayashi Y, et al. Neurodegeneration augments the ability of bone marrow-derived mesenchymal stem cells to fuse with Purkinje neurons in Niemann-Pick type C mice. Hum Gene Ther 2005;16:1006–11.

[42] Tomatsu S, Gutierrez M, Nishioka T, Yamada M, Yamada M, Tosaka Y, et al. Development of MPS IVA mouse (Galnstm(hC79S. mC76S)slu) tolerant to human N-acetylgalactosamine-6-sulfate sulfatase. Hum Mol Genet 2005;14:3321–5.

[43] Matzner U, Matthes F, Herbst E, Lüllmann-Rauch R, Callaerts-Vegh Z, D'Hooge R, et al. Induction of tolerance to human arylsulfatase A in a mouse model of metachromatic leukodystrophy. Mol Med 2007;13:471–9.
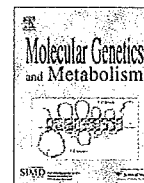
Inhibition of autophagosome formation restores mitochondrial function in mucolipidosis II and III skin fibroblasts

Takanobu Otomo [a,1], Katsumi Higaki [b,1], Eiji Nanba [b], Keiichi Ozono [a], Norio Sakai [a,*]

[a] Department of Pediatrics (D-5), Osaka University Graduate School of Medicine, 2-2 Yamadaoka, Suita, Osaka 565-0871, Japan
[b] Division of Functional Genomics, Research Center for Bioscience and Technology, Tottori University, 86 Nishi-cho, Yonago 683-8503, Japan

ARTICLE INFO

ABSTRACT

Mucolipidosis II and III are progressive lysosomal storage disorders caused by a deficiency of N-acetylglucosamine-1-phosphotransferase, leading to massive accumulation of undigested substrates in lysosomes (inclusion bodies) in skin fibroblast. In this study, we demonstrated accumulation of autolysosomes and increased levels of p62 and ubiquitin proteins in cultured fibroblasts. These autophagic elevations were milder in mucolipidosis III compared with mucolipidosis II. Mitochondrial structure was fragmented and activity was impaired in the affected cells, and 3-methyladenine, an inhibitor of autophagosome formation, restored these. These results show for the first time autophagic and mitochondrial dysfunctions in this disorder.

© 2009 Elsevier Inc. All rights reserved.

1. Introduction

Mucolipidosis (ML)[2] II and III are autosomal recessive diseases caused by a deficiency of UDP-N-acetylglucosamine:lysosomal enzyme N-acetylglucosamine-1-phosphotransferase (GlcNAc-phosphotransferase) and is characterized clinically by developmental delay and dysostosis multiplex, which overlap partially with mucopolysaccharidoses [1]. GlcNAc-phosphotransferase is composed of six subunits $\alpha_2\beta_2\gamma_2$. The α and β subunits are encoded by a single gene GNPTAB and the γ subunit by GNPTG [2,3]. Mutations in GNPTAB cause both severe type ML (ML II alpha/beta, MIM #252500) and attenuated type ML (ML III alpha/beta, MIM #252600), and mutations in GNPTG cause only attenuated type ML (ML III gamma, MIM #252605) [3–6]. GlcNAc-phosphotransferase acts in the first step of synthesizing the mannose 6 phosphate (M6P) recognition marker on lysosomal enzyme proteins, which is recognized by M6P receptor for targeting to the lysosome [7]. In ML patients, lysosomal enzymes lack M6P residues and are hypersecreted into the extracellular space and body fluids instead of being targeted to the lysosome. One of the most characteristic features of these diseases is the presence of numerous phase-dense "inclusion bodies" in

patients' skin fibroblasts, which are thought to be lysosomes filled with undigested compounds. However, their contribution to the pathology of ML II and III are still unclear.

Macroautophagy (hereafter referred to as autophagy) is a lysosomal degradation pathway that is essential for cellular survival [8]. Autophagy not only provides nutrients during fasting but also maintains inner cellular routine turnover by degrading misfolded proteins and damaged organelles such as mitochondria, peroxisomes and endoplasmic reticulum. Recent reports show abnormal lysosomal storage blocks the autophagy pathway and the ubiquitin pathway in lysosomal storage diseases [9,10], but the connection between inclusion body formation and the autophagy pathway in ML II and III cells is not known. In this study we found accumulation of autolysosomes followed by mitochondrial dysfunction in ML fibroblasts, and impaired mitochondrial function was restored by 3-MA, an inhibitor of autophagosome formation. Moreover, these autophagic aberrations indicated some correlation with the severity of clinical phenotypes.

2. Materials and methods

2.1. Cell culture

Human skin fibroblasts from a normal control and ML II, ML III patients were cultured in Dulbecco's modified Eagle's medium (DMEM) supplemented with 10% fetal bovine serum (FBS) and Antibiotic–Antimycotic (GIBCO, Grand Island, NY, USA) with the informed consent of patients. ML II skin fibroblasts had homozygous mutation of c.3565C > T (p.R1189X) in the GNPTAB gene,

---

* Corresponding author. Tel.: +81 6 6879 3932; fax: +81 6 6879 3939.
 E-mail address: norio@ped.med.osaka-u.ac.jp (N. Sakai).
[1] These authors contributed equally to this work.
[2] Abbreviations used: ML, mucolipidosis; GlcNAc-phosphotransferase, UDP-N-acetylglucosamine:lysosomal enzyme N-acetylglucosamine-1-phosphotransferase; M6P, mannose 6 phosphate; LC3, microtubule-associated protein 1 light chain 3; Lamp-2, lysosomal associated membrane protein-2; 3-MA, 3-methyladenine; DMEM, Dulbecco's modified Eagle's medium; PBS, phosphate-buffered saline; BSA, bovine serum albumin; Ub, ubiquitin.

and ML III had compound heterozygote mutations of c.1120T > C (p.F374L) and c.3565C > T (p.R1189X) in the *GNPTAB* gene. These mutations are common in Japanese patients, as reported in the previous paper [11].

2.2. Antibodies and reagents

Polyclonal anti-LC3 (PD014), polyclonal anti-p62/SQSTM1 (PM045) (MBL Co. Ltd., Nagoya, Japan), polyclonal anti-beclin-1 (H-300), monoclonal anti-Ub (P4D1), polyclonal anti-β-tubulin (H-235), monoclonal anti-Lamp-2 (H4B4), polyclonal anti-cathepsin B (S-12), polyclonal anti-cathepsin D (H-75) (Santa Cruz Biotech. Inc., Santa Cruz, CA, USA), monoclonal anti-Tim23 (611223) (BD Biosciences, San Jose, CA, USA), monodansylcadaverine (MDC), and 3-methyladenine (3-MA) (Sigma–Aldrich, St. Louis, MO, USA) were purchased.

2.3. Protein extraction and immunoblotting

Protein extraction from cultured human skin fibroblasts and immunoblotting was performed as described previously [12]. Briefly, equal amounts of proteins (10–20 μg) were electrophoresed in acrylamide gels and subjected to immunoblotting. After incubation with HRP-conjugated secondary antibodies, the membranes were developed using ECL plus reagent (GE Healthcare) and images were captured using X-ray film (RX-U; Fujifilm Co., Tokyo, Japan).

2.4. Fluorescence staining and microscopy

Immunofluorescence staining was performed as described previously [12]. Briefly, cells on coverslips were incubated with primary antibodies against LC3 (1:100), Lamp-2 (1:100), beclin-1 (1:100), ubiquitin (1:100), p62 (1:500), or Tim23 (1:100) for 60 min at room temperature (RT) or 4 °C overnight, and bound antibodies were detected using Alexa Fluor-conjugated secondary antibodies (1:2000 dilution with 0.1% BSA in PBS) for 60 min at RT. For autophagic vacuole labeling, cells were incubated with 50 μM MDC for 10 min at 37 °C. For lysosome staining, cells were incubated with LysoTracker Red DND-99 (100 nM, Molecular Probes Inc., Eugene, OR, USA) for 60 min at 37 °C. For mitochondria staining, cells were incubated with MitoTracker Red CMXRos (100 nM, Molecular Probes Inc.) or JC-1 (3 μM, Molecular Probes Inc.) for 20 min at 37 °C. All fluorescence images were acquired using a fluorescence microscope (Leica DMIRE2; Leica Microsystems, Wetzlar, Germany) or a confocal laser scan microscopy system (Leica TCS SP-2; Leica Microsystems).

2.5. Cathepsin B enzyme activity

The activity of cathepsin B was measured using Magic Red Cathepsin B detection kit (Immunochemistry Tech. LLC, Bloomington, MN, USA). Briefly, cells were prepared on the 96-well cultured plate and incubated with fluorogenic substrate for cathepsin B (MR-(RR)$_2$). Fluorescence was measured using a fluorescence mul-
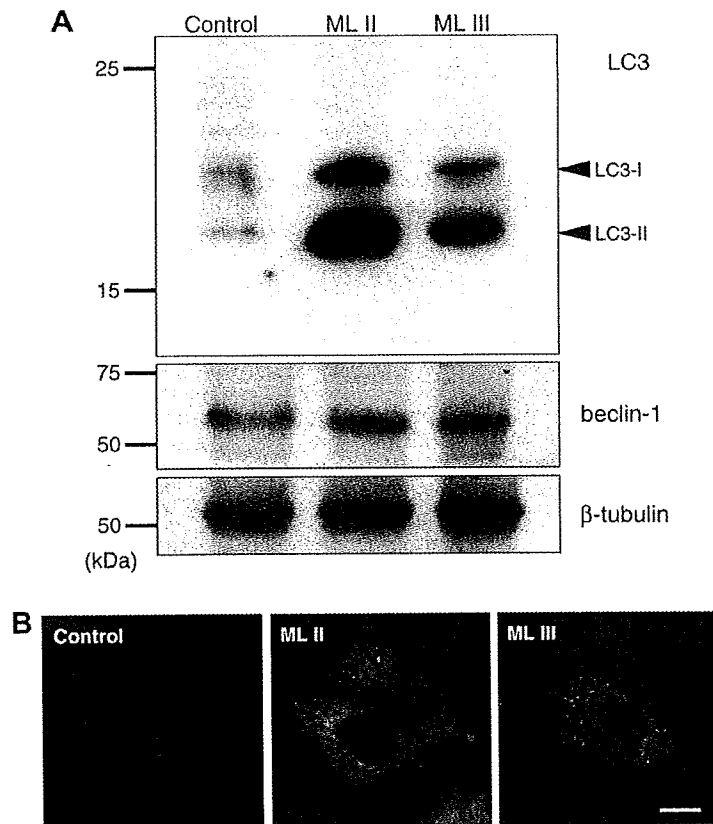

Fig. 1. Elevation of autophagosome formation in ML fibroblasts. (A) Anti-LC3 and beclin-1 immunoblotting of lysates from control, ML II and ML III skin fibroblasts. Densitometric image analysis shows 1.479, 13.862 and 9.672 for LC3-II/LC3-I (average intensities of at least two independent examinations), and 1.028, 0.938 and 0.954 for beclin-1/β-tubulin (average intensities of at least three independent examinations), in control, ML II and ML III, respectively. (B) MDC staining. (C and D) Immunofluorescence of cellular distribution of LC3 with LysoTracker (C) and LC3 with Lamp-2 (D). Bar = 10 μm.
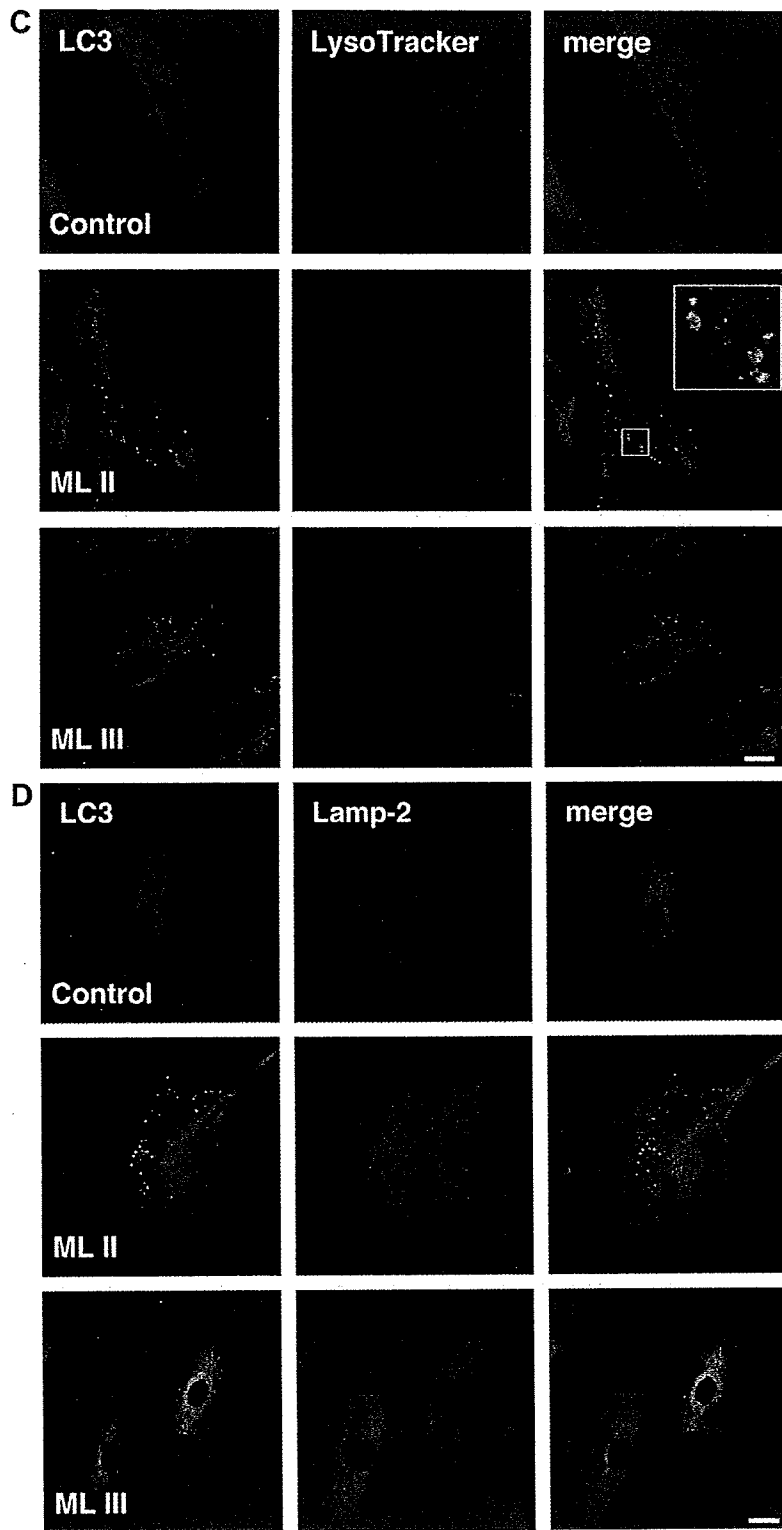
C

LC3	LysoTracker	merge
Control		
ML II		
ML III		

D

LC3	Lamp-2	merge
Control		
ML II		
ML III		

Fig. 1 (continued)

A

Control | ML II | ML III

75 —

50 —

p62

50 —

β-tubulin

(kDa)

B

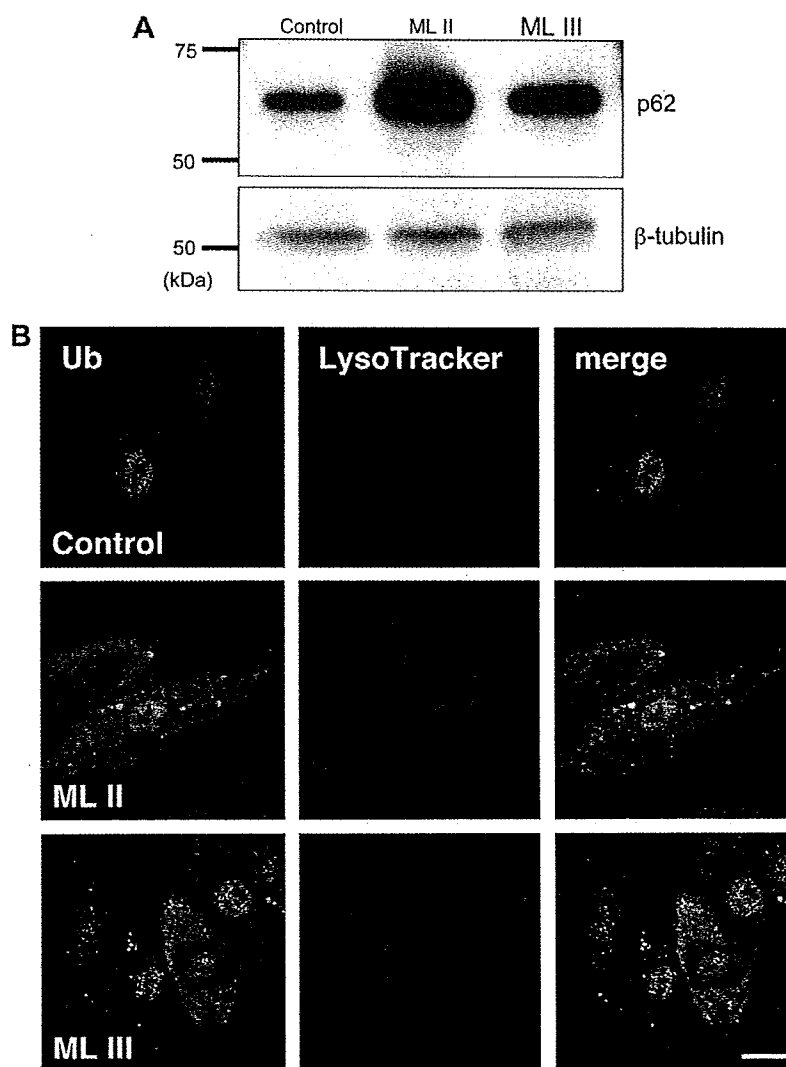| Ub | LysoTracker | merge |

Control

ML II

ML III

Fig. 2. Accumulation of p62 and ubiquitin-positive inclusions in ML fibroblasts. (A) Immunoblotting analysis with anti-p62. (B) Immunofluorescence showed significant accumulation of ubiquitin-positive inclusions colocalized with LysoTracker in ML cells. Bar = 10 μm.

A

Control | ML II | ML III

B
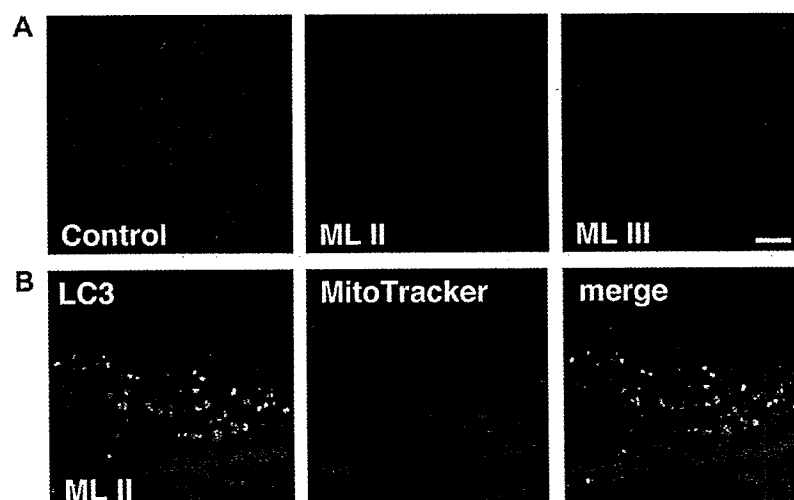
| LC3 | MitoTracker | merge |

ML II

Fig. 3. Mitochondrial impairments in ML fibroblasts. (A) Morphological analysis with MitoTracker-labeled mitochondria. (B) Fluorescence staining with anti-LC3 and MitoTracker revealed that the proportion of tubular-shaped mitochondria was decreased in LC3-positive vesicle rich regions in ML cells. Bar = 10 μm.

ti-well plate reader (excitation 550 nm/emission 640 nm; PerSeptive Biosystems, Framingham, MA, USA).

3. Results

3.1. Increase in autophagosomes and autolysosomes in ML fibroblasts

First, the level of autophagy was assessed in ML fibroblasts. Using Western blotting analysis, the level of LC3-II protein, a membrane bound specific autophagosome marker [8], was found to be increased markedly in the lysate from ML II fibroblasts compared with that in control fibroblasts (Fig. 1A). A modest increase in LC3-II expression was also observed in the lysate from ML III cells. However, the level of beclin-1, a regulator of autophagy, was not elevated in ML II or III cells. The elevation of autophagosome formation was consistent with the observation in ML fibroblasts labeled with MDC, a selective marker for autolysosomes (Fig. 1B). The subcellular localization of autophagosomes was examined using confocal microscopy, and it was found that the number of LC3-positive structures was increased in the cytosol of ML II and III cells, and these LC3-positive structures, especially large vesicles, partly colocalized with LysoTracker and Lamp-2 positive vesicles (Fig. 1C and D). These large circular LC3-positive structures were often seen in ML II cells compared with control and ML III cells.

3.2. Accumulation of ubiquitinated proteins and p62 proteins in ML skin fibroblasts

Recently, p62 protein has been suggested to interact with ubiquitinated proteins and LC3, which may regulate the selective autophagic clearance of protein aggregates [13]. Next, we examined the levels of p62 and ubiquitinated proteins. Immunoblotting analysis showed p62 protein accumulated in the lysates from ML fibroblasts (Fig. 2A). Immunostaining confirmed that ubiquitin (Ub)-positive aggregates were co-labeled with LysoTracker-positive structures in ML cells (Fig. 2B).

3.3. Mitochondrial dysfunction and its restoration by inhibition of autophagy in ML II and III fibroblasts

Autophagic delivery to lysosomes has been shown to be the major pathway in mitochondrial turnover [8]. It was hypothesized that constitutive activation of autophagic formation could affect mitochondrial turnover and impair its function. To address this hypothesis, morphological analysis was performed using MitoTracker Red CMXRos, a membrane potential-dependent fluorescent dye. As shown in Fig. 3A, thick tubular structures of mitochondria were stained by MitoTracker in control cells, whereas thinner tubules and fragmented structures were observed ML II and III fibroblasts (Fig. 3A). These results were the same as in the previous report [14]. When cells were stained using MitoTracker and anti-LC3, MitoTracker-positive tubular structures were decreased near LC3-positive granules in the cytosol of ML fibroblasts, although these did not colocalize (Fig. 3B).

To determine whether the suppression of autophagy recover mitochondrial impairments in ML cells, the effect of 3-MA, an inhibitor of autophagosome formation [15], on ML skin fibroblasts was investigated. When cells were treated with 5 mM 3-MA for 16 h, MitoTracker-labeled mitochondria morphology showed no significant difference from the control cells, whereas thin or fragmented mitochondria seemed to be restored in ML cells (Fig. 4A). Impaired mitochondrial membrane potentials in the affected cells were repeatedly confirmed by staining with JC-1, another mitochondrial membrane sensor, and they recovered significantly after incubation with 3-MA (Fig. 4B).

3.4. Cathepsin B and D in ML II and III fibroblasts

In normal human fibroblasts, cathepsin B and D proteins were transported from the Golgi complex to the lysosome via M6P-dependent pathway [7]. Immunofluorescence analysis showed that cathepsin B and D proteins were colocalized with Lamp-2-positive structures in control fibroblast, whereas these proteins were observed diffuse and partly in the perinuclear, Golgi patterns
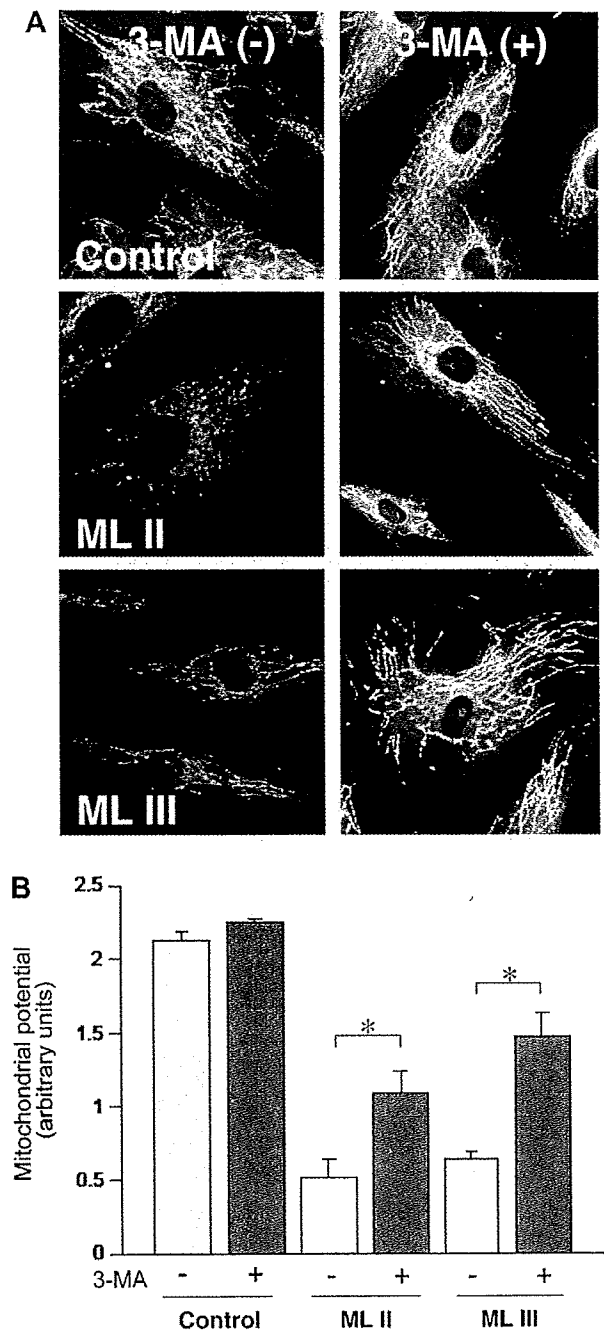

Fig. 4. Restoration of mitochondrial activity by autophagosome inhibitor. Cells were cultured with or without 5 mM 3-MA for 16 h and stained using MitoTracker. DMSO was used as a vehicle (A) MitoTracker staining. (B) The ratio of green and red fluorescence was determined from 10 independent images each of JC-1 labeled-cells. Values are means ± SEM by paired t-test. $p < 0.05$.

(Fig. 5A). The activity of cathepsin B clearly decreased in ML II and III cells, compared to the control (Fig. 5B). Inhibition of autophagy by 3-MA had no effects on subcellular localization of cathepsin B and D proteins (data not shown) and the activity of cathepsin B.

4. Discussion

In this study, accumulation of autolysosomes was observed in ML II and III skin fibroblasts using immunoblotting analysis and immunostaining with anti-LC3. Colocalization studies with LC3, LysoTracker, and Lamp-2 showed that fusion of autophagosomes with late endosomes/lysosomes was not blocked in ML cells. In addition, the accumulation of p62 and ubiquitinated proteins in ML cells suggested a decreased ability to degrade endogenous substrates for autophagy. These findings indicated the impairment of the clearance of autolysosomes in ML II and III skin fibroblasts. Autophagic impairments have been reported in other lysosomal storage disorders [16]. However, the induction of autophagy (marked by beclin-1 activation) differs between these diseases. Elevation of beclin-1 expression has been observed in several cholesterol and sphingolipid storage diseases [17] but not in ML II and

III skin fibroblasts. Beclin-1 is thought to be a positive regulator of the autophagic pathway and it has been shown recently to have multiple functions by forming three different complexes with Vps34 [18]. ML II and III skin fibroblasts have many inclusion bodies filled with undegraded substrates, and these contents have been partially characterized [19]. It is possible that these storage materials complicatedly involves in the downstream pathways of autophagy.

Autophagy is a degradative pathway with major roles in the quality control of bulk cytosolic organelles at steady state [8]. In the present study, the numbers of enlarged vesicles, regarded as autolysosomes, increased remarkably in affected cells. Mitochondrial fragmentation and loss of membrane potential was observed in ML cells, and mitochondrial structure seemed to be excluded especially in autolysosome rich regions from the morphological results. There was a possibility that mitochondria are directly impaired by increased autophagosome formation, because inhibiting the formation of autophagosomes by treating with 3-MA for 16 h lead to the recovery of mitochondrial structure and membrane potential. Mitochondrial impairment in lysosomal storage diseases is considered as a secondary accumulation of
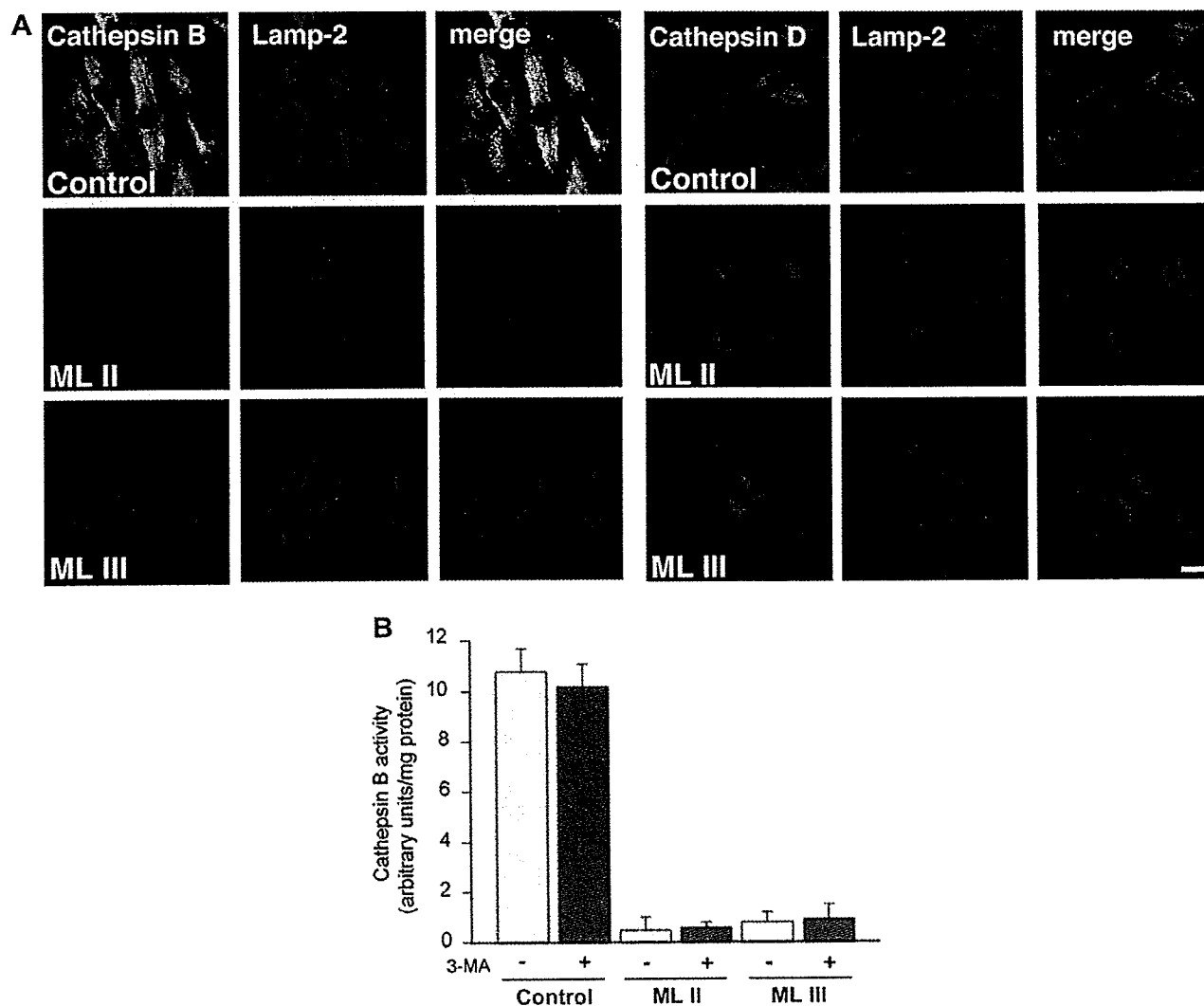

Fig. 5. Subcellar localization and activities of cathepsin B and D. (A) Immunofluorescence of cellular distribution of cathepsin B and D with Lamp-2. Bar = 10 μm. (B) Enzyme activity for cathepsin B. Values are means ± SEM by paired t-test.

abnormal mitochondria caused by the defective autophagic degradation pathways [16]. It is suggested that temporary mitochondrial recovery by blocking autophagy finally results in mitochondrial dysfunction over long periods through the secondary accumulation of abnormal mitochondria followed by cell death.

Cathepsin B and D are the main lysosomal aspartic proteases, which are translocated from the Golgi complex to the late endosomes and lysosomes via M6P-dependent manner [20]. In this study we showed defective cathepsin B and D in ML fibroblasts. Previous studies have reported that autophagy was involved in the pathogeneis of the mouse model of neuronal ceroid lipofuscinoses, which is caused by the mutation in cathepsin D or B/L gene [21]. We propose that the mechanism leading to autophagosome accumulation in ML fibroblasts may at least in part share the common pathway in neuronal ceroid lipofuscinoses. It is also indicated that the 3-MA effect to mitochondria is not derived from the restored cathepsins' activities nor normalization of targeting of cathepsins to lysosomes.

Mitochondrial dysfunction is associated with neurodegenerative and neuromuscular diseases [22,23]. According to these pathological conditions, mitochondrial dysfunction ultimately leads to apoptosis. However, cytochrome-c oxidase deficiency, aberrant mTOR signaling, or active cell death were not detected in steady state cultures of ML cells (data not shown), probably because cultured fibroblasts can dilute accumulating cytosolic contents by cell division. On the other hand, ML skin fibroblasts show very low viability against freezing stock. There is a possibility that mitochondrial function is partially compensated for by regular cell proliferation. Further studies are essential to examine the physiological relevance of these results in ML.

Furthermore, it was also found that the elevated levels of LC3, p62, and ubiquitinated proteins correlated with the clinical findings, though lysosomal enzyme activities or phosphotransferase activities did not correlate with the clinical phenotypes [24]. Recently, enzyme replacement therapy and bone marrow transplantation have been developed as possible therapies for lysosomal storage disorders [25,26]. The present findings may provide significant new insights regarding cellular phenotype and clinical phenotype correlations.

In conclusion, the present provides the first characterization of autophagic impairments accompanied by mitochondrial alterations in cultured ML II and III skin fibroblasts and these impairments were temporarily rescued by blocking autophagy. These findings raise the possibility of exploring new therapeutic options by modulating of inclusion body formation and autophagic impairments in ML II and ML III patients.

Acknowledgments

References

[1] S. Kornfeld, W.S. Sly, I-cell disease and pseudo-hurler polydystrophy: disorders of lysosomal enzyme phosphorylation and localization, in: C.R. Scriver, A.L. Beaudet, W.S. Sly, D. Valle (Eds.), The Metabolic and Molecular Bases of Inherited Disease, McGraw-Hill, New York, 2001, pp. 3469–3482.

[2] M. Kudo, M. Bao, A. D'Souza, F. Ying, H. Pan, B.A. Roe, W.M. Canfield, The alpha- and beta-subunits of the human UDP-N-acetylglucosamine:lysosomal enzyme N-acetylglucosamine-1-phosphotransferase are encoded by a single cDNA, J. Biol. Chem. 280 (2005) 36141–36149.

[3] A. Raas-Rothschild, V. Cormier-Daire, M. Bao, E. Genin, R. Salomon, K. Brewer, M. Zeigler, H. Mandel, S. Toth, B. Roe, A. Munnich, W.M. Canfield, Molecular basis of variant pseudo-hurler polydystrophy (mucolipidosis IIIC), J. Clin. Invest. 105 (2000) 673–681.

[4] S. Tiede, S. Storch, T. Lübke, B. Henrissat, R. Bargal, A. Raas-Rothschild, T. Braulke, Mucolipidosis II is caused by mutations in GNPTA encoding the alpha/betaGlcNAc-1-phosphotransferase, Nat. Med. 11 (2005) 1109–1112.

[5] M. Kudo, M.S. Brem, W.M. Canfield, Mucolipidosis II (I-cell disease) and mucolipidosis IIIA (classical pseudo-hurler polydystrophy) are caused by mutations in the GlcNAc-phosphotransferase alpha /beta-subunits precursor gene, Am. J. Hum. Genet. 78 (2006) 451–463.

[6] K.H. Paik, S.M. Song, C.S. Ki, H.W. Yu, J.S. Kim, K.H. Min, S.H. Chang, E.J. Yoo, I.J. Lee, E.K. Kwan, S.J. Han, D.K. Jin, Identification of mutations in the GNPTA (MGC4170) gene coding for GlcNAc-phosphotransferase alpha/beta subunits in Korean patients with mucolipidosis type II or type IIIA, Hum. Mutat. 26 (2005) 308–314.

[7] T. Braulke, J.S. Bonifacino, Sorting of lysosomal proteins, Biochim. Biophys. Acta 1793 (2009) 605–614.

[8] N. Mizushima, Autophagy: process and function, Genes Dev. 21 (2007) 2861–2873.

[9] C. Settembre, A. Fraldi, L. Jahreiss, C. Spampanato, C. Venturi, D. Medina, R. de Pablo, C. Tacchetti, D.C. Rubinsztein, A. Ballabio, A block of autophagy in lysosomal storage disorders, Hum. Mol. Genet. 17 (2008) 119–129.

[10] P. Bifsha, K. Landry, L. Ashmarina, S. Durand, V. Seyrantepe, S. Trudel, C. Quiniou, S. Chemtob, Y. Xu, R.A. Gravel, R. Sladek, A.V. Pshezhetsky, Altered gene expression in cells from patients with lysosomal storage disorders suggests impairment of the ubiquitin pathway, Cell Death Differ. 14 (2007) 511–523.

[11] T. Otomo, T. Muramatsu, T. Yorifuji, T. Okuyama, H. Nakabayashi, T. Fukao, T. Ohura, M. Yoshino, A. Tanaka, N. Okamoto, K. Inui, K. Ozono, N. Sakai, Mucolipidosis II and II alpha/beta: mutation analysis of 40 Japanese patients showed genotype–phenotype correlation, J. Hum. Genet. 54 (2009) 145–154.

[12] A. Takamura, K. Higaki, K. Kajimaki, S. Otsuka, H. Ninomiya, J. Matsuda, K. Ohno, Y. Suzuki, E. Nanba, Enhanced autophagy and mitochondrial aberrations in murine GM1-gangliosidosis, Biochem. Biophys. Res. Commun. 367 (2008) 616–622.

[13] Y. Ichimura, T. Kumanomidou, Y.S. Sou, T. Mizushima, J. Ezaki, T. Ueno, E. Kominami, T. Yamane, K. Tanaka, M. Komatsu, Structural basis for sorting mechanism of p62 in selective autophagy, J. Biol. Chem. 283 (2008) 22847–22857.

[14] J.J. Jennings, J.-H. Zhu, Y. Rbaibi, X. Luo, C.T. Chu, K. Kiselyov, Mitochondrial aberrations in mucolipidosis type IV, J. Biol. Chem. 281 (2006) 39041–39050.

[15] P.O. Seglen, P.B. Gordon, 3-Methyladenine: specific inhibitor of autophagic/lysosomal protein degradation in isolated rat hepatocytes, Proc. Natl. Acad. Sci. USA 79 (1982) 1889–1892.

[16] A. Ballabio, V. Gieselmann, Lysosomal disorders: from storage to cellular damage, Biochim. Biophys. Acta 1793 (2009) 684–696.

[17] C.D. Pacheco, R. Kunkel, A.P. Lieberman, Autophagy in Niemann–Pick C disease is dependent upon Beclin-1 and responsive to lipid trafficking defects, Hum. Mol. Genet. 16 (2007) 1495–1503.

[18] K. Matsunaga, T. Saitoh, K. Tabata, H. Omori, T. Satoh, N. Kuratori, I. Maejima, K. Shirahama-Noda, T. Ichimura, T. Isobe, S. Akira, T. Noda, T. Yoshimori, Two Beclin 1-binding proteins, Atg14L and Rubicon, reciprocally regulate autophagy at different stages, Nat. Cell Biol. 11 (2009) 385–396.

[19] I. Kawashima, M. Ohsawa, T. Fukushige, Y. Nagayama, Y. Niida, M. Kotani, Y. Tajima, T. Kanekura, T. Kanzaki, H. Sakuraba, Cytochemical analysis of storage materials in cultured skin fibroblasts from patients with I-cell disease, Clin. Chim. Acta 378 (2007) 142–146.

[20] S. Tiede, N. Muschol, G. Reutter, M. Cantz, K. Ullrich, T. Braulke, Missense mutations in N-acetylglucosamine-1-phosphotransferase alpha/beta subunit gene in a patient with mucolipidosis III and a mild clinical phenotype, Am. J. Med. Genet. A 137 (2005) 235–240.

[21] M. Koike, M. Shibata, S. Waguri, K. Yoshimura, I. Tanida, E. Kominami, T. Gotow, C. Peters, K. von Figura, N. Mizushima, P. Saftig, Y. Uchiyama, Participation of autophagy in storage of lysosomes in neurons from mouse models of neuronal ceroid-lipofuscinoses (Batten disease), Am. J. Pathol. 167 (2005) 1713–1728.

[22] A.B. Knott, G. Perkins, R. Schwarzenbacher, E. Bossy-Wetzel, Mitochondrial fragmentation in neurodegeneration, Nat. Rev. Neurosci. 9 (2008) 505–518.

[23] A.H. Schapira, Mitochondria in the aetiology and pathogenesis of Parkinson's disease, Lancet Neurol. 7 (2008) 97–109.

[24] S. Okada, M. Owada, T. Sakiyama, T. Yutaka, M. Ogawa, I-cell disease: clinical studies of 21 Japanese cases, Clin. Genet. 28 (1985) 207–215.

[25] S. Grewal, E. Shapiro, E. Braunlin, L. Charnas, W. Krivit, P. Orchard, C. Peters, Continued neurocognitive development and prevention of cardiopulmonary complication after successful BMT for I-cell disease: a long-term follow-up report, Bone Marrow Transplant. 32 (2003) 957–960.

[26] M. Beck, New therapeutic options for lysosomal storage disorders: enzyme replacement, small molecules and gene therapy, Hum. Genet. 121 (2007) 1–22.

The transcriptional repressor RP58 is crucial for cell-division patterning and neuronal survival in the developing cortex

Haruo Okado [a,*,1,2,3], Chiaki Ohtaka-Maruyama [a,1,2,4], Yoshinobu Sugitani [b,1,2,4], Yuko Fukuda [c,2], Reiko Ishida [c,2], Shinobu Hirai [a,2], Akiko Miwa [a,2], Akiyo Takahashi [a,2], Katsunori Aoki [d,2], Keiji Mochida [e,2,4], Osamu Suzuki [f,4], Takao Honda [g,2], Kazunori Nakajima [g,4], Masaharu Ogawa [b,4], Toshio Terashima [h,4], Junichiro Matsuda [f,2,5], Hitoshi Kawano [i,1,4], Masataka Kasai [c,1]

[a] Department of Molecular Physiology, Tokyo Metropolitan Institute for Neuroscience, 2-6 Musashidai, Fuchu, Tokyo 183-8526, Japan
[b] Ogawa research unit, Neuro-developmental disorder research group, Brain Science Institute, Riken, Saitama 351-0198, Japan
[c] Department of Immunology, National Institute of Infectious Diseases, 1-23-1 Toyama, Shinjuku-ku, Tokyo 162-8640, Japan
[d] Department of Hematology (Internal Medicine), The University of Tokyo, Bunkyo-ku, Tokyo 113-8655, Japan
[e] Bioresource Center, RIKEN, Tsukuba, Ibaraki 305-0074, Japan
[f] Department of Veterinary Science, National Institute of Infectious Diseases, 1-23-1 Toyama, Shinjuku-ku, Tokyo 162-8640, Japan
[g] Department of Anatomy, Keio University School of Medicine, Tokyo 160-8582, Japan
[h] Division of Anatomy and Developmental Neurobiology, Department of Neuroscience, Kobe University Graduate School of Medicine, Kobe 650-0017, Japan
[i] Department of Developmental Morphology, Tokyo Metropolitan Institute for Neuroscience, 2-6 Musashidai, Fuchu, Tokyo 183-8526, Japan

ARTICLE INFO

ABSTRACT

The neocortex and the hippocampus comprise several specific layers containing distinct neurons that originate from progenitors at specific development times, under the control of an adequate cell-division patterning mechanism. Although many molecules are known to regulate this cell-division patterning process, its details are not well understood. Here, we show that, in the developing cerebral cortex, the RP58 transcription repressor protein was expressed both in postmitotic glutamatergic projection neurons and in their progenitor cells, but not in GABAergic interneurons. Targeted deletion of the RP58 gene led to dysplasia of the neocortex and of the hippocampus, reduction of the number of mature cortical neurons, and defects of laminar organization, which reflect abnormal neuronal migration within the cortical plate. We demonstrate an impairment of the cell-division patterning during the late embryonic stage and an enhancement of apoptosis of the postmitotic neurons in the RP58-deficient cortex. These results suggest that RP58 controls cell division of progenitor cells and regulates the survival of postmitotic cortical neurons.

© 2009 Elsevier Inc. All rights reserved.

Introduction

Glutamatergic cortical neurons are generated from progenitor cells in the cortical germinal zone and migrate radially in an inside-to-outside gradient. The earliest neurons form the preplate (together with the Cajal-Retzius cells) and the neurons born subsequently migrate past the earliest-born neurons to intercalate within the preplate, divide it into the marginal zone (MZ; layer 1) and the subplate (layer 6b), and form the lower layers of the cortical plate

* Corresponding author.
E-mail address: hokado@rinn.ac.jp (H. Okado).
[1] H.O. C.O-M. Y.S. H.K. and M.K. designed the research.
[2] H.O. C.O-M, Y.S., Y.F., R.I., S.H., A.M., A.T., K.A., K.M., T.H., J.M. performed the research.
[3] H.O. wrote the paper.
[4] C.O-M, Y.S., O.S., K.N., M.O. T.T. H.K., K.M provided helpful discussion and guidance
[5] Present address: National Institute of Biomedical Innovation, Ibaraki City, Osaka 567-0085, Japan.

(CP). Late-born neurons then migrate past the early-born neurons to form the upper layers of the CP, beneath the MZ. In contrast, GABAergic neurons and Cajal-Retzius cells are generated from progenitor cells outside the neocortex, in the ganglion eminence and in the cortical hem, respectively, and migrate tangentially into the neocortex (Bayer and Altman, 1991; Allendoerfer and Shatz, 1994; Molyneaux et al., 2007). The radial glial progenitors (RGPs) in the ventricular zone (VZ) give rise to cortical neurons, while the progenitor cells in the subventricular zone (SVZ) produce a substantial number of upper-layer neurons (Smart and McSherry, 1982, Tarabykin et al., 2001, Sugitani et al., 2002). Some of the SVZ progenitor cells are intermediate progenitors (IMPs), which originate from the VZ and produce neurons by dividing limited times (Noctor et al., 2004, Haubensak et al., 2004, Miyata et al., 2004). In the hippocampus, pyramidal neurons of the Cornu Ammonis (CA) are generated from the VZ of the hippocampus, whereas the precursors of the granular neurons of the dentate gyrus (DG) originate in the neuroepithelium near the cortical hem, migrate towards the anlage of

the DG, continue to divide, and undergo further migration to the granule layer of the DG (Forster et al., 2006. Li and Pleasure 2007).

These cortical progenitor cells generate a vast diversity of terminally differentiated neuronal phenotypes. The balance between exit from and reentry into the cell cycle is important for the formation of these cell types at appropriate times; however, the molecular mechanism underlying this regulation is not completely understood (Dehay and Kennedy, 2007).

We have previously described a novel DNA binding protein, RP58 (also known as ZNF238), which shares homology with the POZ domain of a number of zinc finger (ZF) proteins, which are termed POZ-ZF proteins (Aoki et al., 1998). RP58 exhibits a sequence-specific transcriptional repressor activity (Aoki et al., 1998) and probably acts by binding to the DNA methyltransferase Dnmt3a, which associates with histone deacetylase and acts as a corepressor (Fuks et al., 2001). POZ-ZFs are important for many biological processes, which include B-cell fate determination, DNA damage responses, cell-cycle progression, and a multitude of developmental events (Kelly and Daniel, 2006). Among the POZ-ZF proteins, the promyelocytic leukemia zinc finger (PLZF) is essential for stem cell self renewal in the murine testis (Buaas et al., 2004; Costoya et al. 2004), Miz1 plays an essential role in the control of the exit from the cell cycle during the hair cycle (Gebhardt et al., 2007), and ZENON is involved in the maintenance of panneuronal features and/or in the survival of mature neurons (Kiefer et al., 2005).

We demonstrated that RP58 transcripts are highly expressed in the cerebral cortex in the embryonic mouse brain (Ohtaka-Maruyama et al., 2007). In addition, RP58 is expressed weakly in the VZ and intensely in the SVZ, intermediate zone (IZ), and CP in the embryonic cortex, which suggests that RP58 is important for the early development of cortical neurons. In adult cerebral cortex, the expression of the RP58 transcript is maintained in glutamatergic neurons, but not in GABAergic neurons.

In the present study, we investigated the role of RP58 in the development of the cerebral cortex by generating and analyzing *RP58*-deficient mice. Our results demonstrate that *RP58* deficiency causes enhanced apoptosis and impairs the cell-division patterning in the VZ during late development, which suggests that RP58 is a novel regulator of glutamatergic neuron survival and of progenitor cell division.

Materials and methods

Generation of RP58-deficient mice

Similarly to what is observed for the human *RP58* gene, the sequence of the mouse *RP58* gene that encodes the functional protein is uninterrupted over its entire 4.2 kb length (Meng et al., 2000). A gene-targeting construct was prepared by deletion of the entire exon (5.4 kb). The resulting *RP58* targeting vector (Supplementary Fig. 1A), which was constructed from a mouse strain 129 library (Stratagene) and consisted of a 4.2 kb homology arm derived from the 5′ end of the exon, a PGK promoter-neomycin expression cassette, and a 2.7 kb homology arm from the 3′ end of the exon, was linearized with XbaI and introduced into GSI ES cells (derived from the 129/SvJ mouse strain) by electroporation. Colonies that survived after selection were picked and expanded for DNA analysis. Targeted ES cells were injected into the blastocoel cavity of C57/BL6 embryos using a piezo-driven micromanipulator (PrimeTech, Tsuchiura, Japan) to generate chimeric mice, which were then crossed with C57/BL6 females to obtain heterozygous *RP58*⁺/⁻ mutant animals. These mice were, in turn, interbred to produce homozygous *RP58*⁻/⁻ mice at the expected Mendelian frequency.

Southern blot analysis of genomic DNA isolated from the tails of embryonic day (E) 18.5 fetuses confirmed the homologous integration of the target vector (Supplementary Fig 1B), which resulted in the replacement of the entire *RP58* exon (5.4 kb) with the neomycin

resistance gene. Northern blot analysis of total RNA extracted from genotyped embryonic brains (Supplementary Fig. 1C) showed that the RP58 transcript was present only in wild-type and heterozygous embryos. In homozygous mutant embryos, no RP58 transcript of any size was observed. Embryonic brain extracts were incubated with anti-RP58-conjugated Sepharose 4B beads. The beads were washed extensively and boiled in SDS sample buffer. After centrifugation, the supernatant was analyzed for the presence of RP58 by immunoblotting, as described previously (Ishida et al., 2002). To confirm the specificity of the interactions between the antigen and the antibody, the peptide (CLPTVRDWTLEDSSQELWK) used for the generation of the anti-RP58 antibody was added during the immunoprecipitation experiment. Antibodies specific to RP58 detected the protein in brain extracts from wild-type, but not homozygous mutant, embryos (Supplementary Fig. 1D). The day after the mating was designated E0.5.

Immunohistochemistry

Heads of embryos were removed, fixed in Bodian's fixative (3.7% formaldehyde, 80% ethanol), embedded in paraffin, and sectioned at an 8 μm thickness. A few embryos were perfused with 4% paraformaldehyde and sectioned using a cryostat (10–25 μm thickness). In most cases, the antigens in these sections were reactivated by heating in 10 mM citrate buffer (adjusted to pH 6.0) using a microwave or an autoclave.

We used the following antibodies: rabbit anti-mouse RP58 (1:500, Takahashi et al., 2008), mouse anti-reelin (1:200, Chemicon), rabbit anti-MAP2 (1:500, Chemicon), rabbit anti-Tbr1 (1:500, Chemicon), rabbit anti-Prox1 (1:1000, Covance), chicken anti-Tuj1 (1:200, Chemicon), mouse anti-BrdU (1:50, Becton-Dickinson), rat anti-BrdU (1:200, Abcam), mouse anti-α-synuclein, mouse anti-β-synuclein (1:200, BD Transduction Lab), rabbit anti-Pax6 (1:200, Chemicon), mouse anti-PCNA (1:200, Chemicon), mouse anti-nestin (1:200, Rat-401), mouse anti-NeuN (1:100, Chemicon), mouse anti-Ki67 (1:100, Novocastra), rabbit anti-Ki67 (1:500, Novocastra), goat anti-NeuroD (1:100, Santa Cruz Biotechnology), guinea pig anti-Dlx2 (1:1000, gift from Dr. Yoshikawa; Kuwajima et al., 2006), mouse anti-Neurogenin2 (1:5, gift from Dr. Anderson), rabbit anti-phosphohistone H3 (P-H3) (1: 200, Upstate), rabbit anti-neurofilament (1:500, Fukuda et al., 1997), rabbit anti-ssDNA (1:400, DAKO), rabbit anti-active caspase 3 (1:400, R&D), and goat anti-Unc5d (1:200, R&D).

Anti-IgG antibodies conjugated to biotin (Vector, 1:200), Alexa 488, Alexa 546, Alexa 555, Cy3, or Cy5 (1:500) (Molecular Probes or Jackson Laboratories) were used as secondary antibodies and the ABC kit (Vector) or the TSA Fluorescence System (PerkinElmer) were used to detect biotin. After nuclear staining with DAPI and Topro3, the sections were mounted with PermaFluor (Immunon) or were dehydrated and mounted with Entellan Neu (Merk). A laser-scanning confocal microscope was used to image fluorescence signals.

To perform RP58/Pax6 and RP58/Tbr2 double labeling using rabbit polyclonal antibodies, we used the TSA or TSA Plus Fluorescence System (PerkinElmer), according to Friocourt et al. (2008). Sections were first incubated with diluted anti-RP58 antibody (1:8000), for the TSA Plus Fluorescence System, and were then incubated with rabbit anti-Pax6 antibody (1:200), anti-Tbr2 antibody (1:200), or no antibody (negative control). For RP58/P-H3 double labeling, sections were first incubated with anti-RP58 antibody (1:500), for the TSA Fluorescence System, and were then incubated with rabbit anti-P-H3 antibody (1:200). For Pax6/Tbr2 double labeling, sections were first incubated with diluted anti-Pax6 antibody (1:30000), for the TSA Plus Fluorescence System, and were then incubated with rabbit anti-Tbr2 antibody (1:200). For Pax6/Tbr2/Unc6d triple labeling, sections were first incubated with diluted anti-Pax6 antibody (1:15000), for the TSA Plus Fluorescence System, and were then incubated with rabbit anti-Tbr2 (1:200) and anti-Uncd5 (1:200) antibodies.

RNA in situ hybridization

We used single-stranded digoxigenin (DIG)-UTP-labeled RNA probes generated from the mouse *RP58* cDNA (approximately 1.6 kb); mouse *ER81* (a gift from Dr. Jessell; Arber et al., 2003); mouse *RORβ* (a gift from Dr. McConnell; Weimann et al., 1999); *Svet1* (a gift from Dr. Tarabykin; Tarabykin et al., 2001); *NT3* (a gift from Dr. Aizawa; Shimozaki et al., 2004); rat *SCIP* (a gift from Dr. Lemke), mouse α-crystalline (a gift from Dr. Funatsu; Funatsu et al., 2004), rat *KA1* (a gift from Dr. Boulter; Better et al., 1990), for mouse *Tbr1*, mouse *mSorLA*, mouse *CTGF*, and mouse *Tailless* (gifts from Drs. Y Sugitani and T Noda; Sugitani et al., 2002); *HES5* cDNA (a gift from Dr. Guillemot; Cau et al., 2000). Some probes were hydrolyzed to a length of about 200–500 bp. RNA *in situ* hybridization was performed on Bodian's-fixed paraffin sections, according to the method of Ohtaka-Maruyama et al. (2007), and on 4% paraformaldehyde-fixed frozen sections, according to the method of Sugitani et al. (2002). In some cases, the counterstaining was performed using Nuclear Fast Red (Kernechtrot).

BrdU- and IdU-labeling experiments

Bromodeoxyuridine (BrdU) or iododeoxyuridine (IdU) (50 mg/kg of body weight) were injected intraperitoneally into pregnant mice at various developmental stages. To estimate the rates of cell-cycle exit, randomly selected BrdU-positive cells (about 50 cells) were examined for PCNA or Pax6 immunoreactivity 24 h after the incorporation of BrdU. In particular, the rates of cell-cycle exit were estimated in the lower region (which corresponded to the VZ) and in the upper region (which corresponded to the SVZ and IZ) of E16.5 embryos in which BrdU was incorporated on E15.5. The total number of BrdU-positive cells was counted and examined for Pax6 immunoreactivity (which corresponds to 0.09 mm of the ventricular surface). The SVZ was identified by staining with Unc5d/Svet1.

To estimate the production of progenitor cells, randomly selected Ki67-positive cells were examined for BrdU immunoreactivity 0.5 h after the incorporation of BrdU.

The estimation of cell-cycle kinetics was performed according to Maruynoga et al. (2005). P$_{cells}$ was estimated by counting the total number of cells in the prospective VZ within the sampling area.

TUNEL assay

Apoptosis was detected using a TUNEL assay kit (Dead End Fluorometric TUNEL system, Promega). Deparaffinized sections were treated with proteinase K (20 μg/ml) in 100 mM Tris-Cl and 50 mM EDTA (pH = 8.0) for 15 min at room temperature (RT), followed by treatment with FITC-nucleotide containing TdT or H$_2$O (as a negative control), and counterstaining using propidium iodide.

Results

Targeted disruption of the RP58 gene

To study the role of RP58 in the development of the central nervous system, we disrupted the *RP58* gene in embryonic stem cells using the target vector (see Supplementary Fig. 1A and "Materials and methods" section). Heterozygous (*RP58*⁺/⁻) mice were phenotypically indistinguishable from their wild-type littermates, whereas all homozygous (*RP58*⁻/⁻) mice, which were generated from intercrosses of the heterozygotes, died shortly after birth. The cause of the death remains unknown and is currently under investigation.

Hypoplasia of the hippocampus and neocortex in RP58-deficient mice

Because RP58 transcripts are expressed abundantly in the brain of the wild-type mice (*RP58*⁺/⁺; Ohtaka-Maruyama et al., 2007) and

RP58⁻/⁻ mice die shortly after birth, we performed histological analyses of brains isolated from null, heterozygous, and wild-type animals at neonatal and embryonic stages. We observed hypoplasia of the neocortex and hippocampus in *RP58*⁻/⁻ mice, whereas the brains of *RP58*⁺/⁻ mice appeared to be normal (Fig. 1; Supplementary Figs. 1E–M). Therefore, we compared *RP58*⁻/⁻ mice with either wild-type or *RP58*⁺/⁻ mice in subsequent experiments. The neocortex of *RP58*⁻/⁻ mice displayed a reduced thickness and its layers were disorganized. Furthermore, the VZ appeared to expand radially in the mutant cortex (asterisk in Fig. 1). In the mutant hippocampus, the pyramidal cell layer and the typical V-shaped granule cell layer of the DG were not evident (Fig. 1). Additionally, the cerebellum of *RP58*⁻/⁻ mice lacked the typical foliation observed in wild-type and heterozygous animals (see Supplementary Figs. 1K–M). In the present study, we focused our analysis on the neocortex and hippocampus of mutant mice.

Reduced numbers of mature neurons in the mutant neocortex and hippocampus

Double staining of the neocortex with MAP2 and β-III-Tubulin (Tuj1) showed that postmitotic neurons were present in the mutant neocortex; however, the subplate layer was incompletely formed in the medial region of the mutant neocortex (arrowheads in Supplementary Figs. 2A–B").

To further characterize this abnormality of the neocortex, we examined the expression of various layer markers. The number of E19 subplate neurons positive for the connective tissue growth factor (CTGF), which labels maturing subplate neurons in layer 6b (Friedrichsen et al., 2003; Heuer et al., 2003), was drastically decreased in the mutant neocortex when compared with the wild type (Figs. 2A and B). To detect the subplate neurons at the earlier stage, we examined the staining for β-synuclein, which is an inhibitor
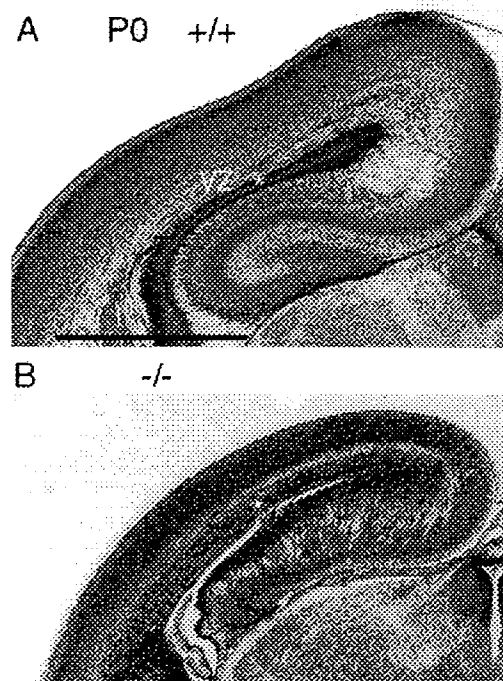

Fig. 1. Defects in brain formation in *RP58*⁻/⁻ mice at P0. Nissl-stained coronal sections of forebrains from (A) wild-type (+/+) and (B) RP58-deficient (−/−) mice showed cytoarchitectural abnormalities in the neocortex and hippocampus of the mutant animal. In the mutant, the thickness of the neocortex was reduced and the ventricular zone (VZ) (marked with an asterisk) was expanded. Cresyl violet staining. Scale bar, 1 mm (A, B).
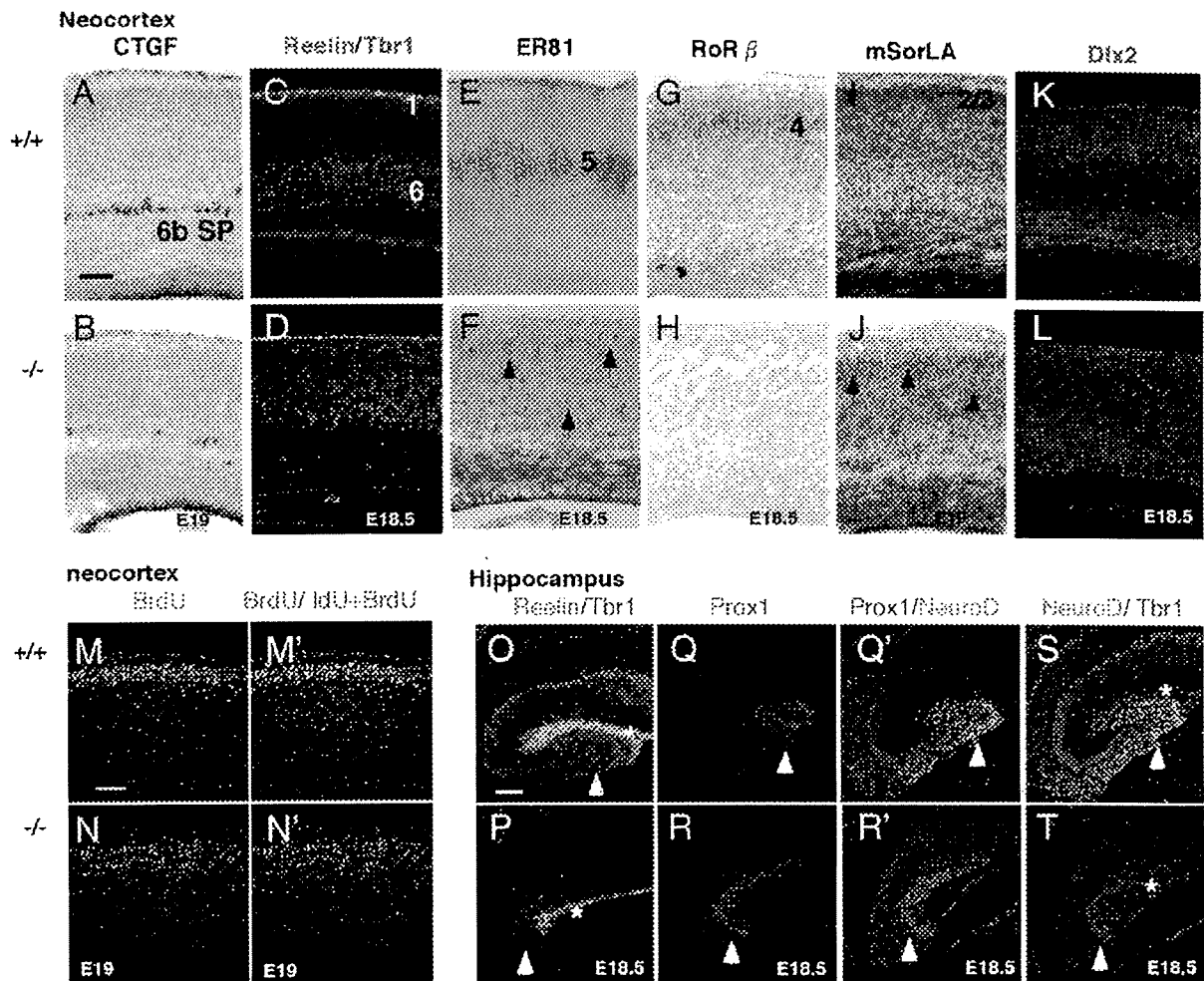
Fig. 2. Dysplasia of the neocortex and hippocampus in RP58⁻/⁻ mice. (A–L) The disorganized laminar structures of the neocortex and hippocampus of the mutant were demonstrated by various layer-specific markers at E19 (A and B) or E18.5 (C–L) in the wild-type (−/−) and RP58-deficient (−/−) neocortex. (A and B) CTGF-labeled subplate neurons, (C and D) reelin-labeled layer 1 Cajal-Retzius neurons and Tbr1-labeled layer 6 cortical neurons, (E and F) ER81-labeled layer 5 cortical neurons, (G and H) RoRβ-labeled layer 4 cortical neurons, (I and J) mSorLA-labeled layer 2/3 cortical neurons, and (K and L) Dlx2-labeled GABAergic neurons. In the mutant neocortex, the subplate neurons were sharply reduced in number (A and B). Cajal-Retzius neurons were normal (C and D). Tbr1-positive cells were shifted more superficially and were more widely scattered when compared with the wild type (C and D). ER81- and mSorLA-positive cells were located diffusely and in reduced numbers (arrows in F and J), the expression level of RoRβ was dramatically reduced (G and H), and Dlx1-positive cells were roughly normal (K and L). Scale bar, 0.1 mm (A–L).

of the aggregation of α-synuclein (Hashimoto et al. 2001), as a marker for subplate neurons. Since β-synuclein is mostly detected in the deepest region of layer 6, identified with Tbr1 immunoreactivity, β-synuclein-positive cells correspond to the subplate neurons in the wild-type cortex at E16.5 (arrows in Supplementary Figs. 2E–E''). In mutant neocortices, the number of subplate neurons was severely reduced and a part of the surviving subplate neurons was displaced superficially at E16.5 (Supplementary Figs. 2C–F). In addition, in the RP58 mutants, a fraction of the neurofilament-positive thalamocortical fibers (Kawano et al. 1999), which use subplate neurons for their pathfinding, abnormally projected towards the surface of the neocortex (Fig 3).

Reelin-positive Cajal-Retzius neurons (Ogawa et al. 1995) developed normally in layer 1 in the E18.5 mutant (Figs. 2C and D, green). In the E18.5 mutant cortex, the majority of the Tbr1-positive cells was located in the deeper part of cortical plate (Fig. 2C; Supplementary Fig. 4E); however, many of these cells were also detected diffusely throughout the CP (Fig. 2D; Supplementary Fig. 3F). ER81, which is a layer 5 marker (Sugitani et al. 2002), was expressed in many cells in the wild-type CP (Fig. 2E); in contrast, this marker was expressed in only a few cells in the E18.5 mutant CP (arrows in Fig. 2F). Cells in the

mutant cortex were only faint positive for RORβ, which labels layer 4 neurons (Weimann et al. 1999) (Figs. 2G and H). mSorLA labels layer 2/3 neurons (Fig. 2I, Sugitani et al. 2002; Hermans-Borgmeyer et al. 1998); mSorLA-positive cells in the mutant cortex were diffusely distributed and dramatically reduced in number (arrows in Fig. 2J). In contrast, GABA-positive (data not shown) and Dlx2-positive (Figs. 2K and L) inhibitory interneurons of the mutant neocortex did not display any distinct abnormalities, although their distribution pattern appeared slightly disturbed. These results suggest that mature subplate neurons and mature CP neurons, which form the future cortical layers 2–5, were reduced in number in RP58⁻/⁻ mice.

The diffuse distribution of Tbr1-positive and other cortical neurons in the mutant cortex raised the possibility that the RP58 deficiency impaired the inside-out layer formation. To examine this possibility, we performed double labeling by injecting iododeoxyuridine (IdU) at E12.5 and 5-bromo-2-deoxyuridine (BrdU) at E14.5, followed by examination of the brains at E19 (Figs. 2M–N'). Most late-born cortical neurons (Figs. 2M' and N', yellow) crossed over early-born cells (Figs. 2M' and N', red) in the wild-type cortex, while many late-born neurons were abnormally located beneath early-born cells in the mutant cortex. The defects of laminar organization observed in the
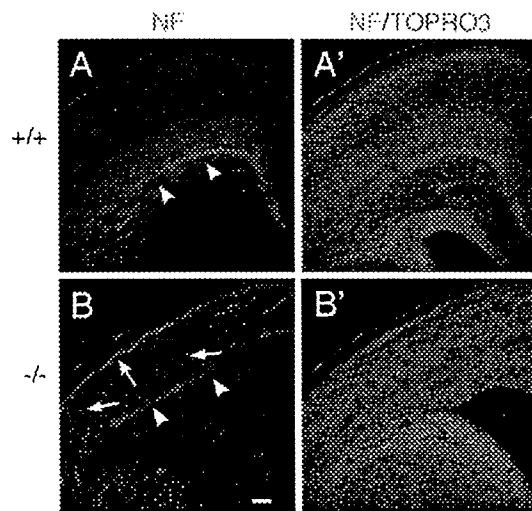
NF   NF/TOPRO3

+/+

-/-

Fig. 3. Abnormality of the thalamocortical pathway formation in the *RP58*-deficient cortex. Coronal sections from E18.5 wild-type (A, A') and *RP58⁻ ⁻* (B, B') brains stained with anti-neurofilament (NF) antibodies and TOPRO3 (nuclear stain) (A', B'). In the wild type, thalamocortical axons that were immunoreactive for neurofilament ran along the subplate beneath the cortical plate (arrowheads in A), while in the *RP58⁻ ⁻* brain, some labeled axons ran along the subplate beneath the cortical plate (arrowheads in B), whereas the other axons invaded the cortical plate towards the pial surface (arrows in B). Scale bar, 0.1 mm (A–B').

RP58 mutant cortices suggest that RP58 may play a role in neuronal positioning or migration.

The *RP58*-deficient hippocampus was reduced in size and had no identifiable CA pyramidal layer or DG granular layer in sections stained with Nissl (Fig. 1), NeuN (Supplementary Figs. 2C' and H'), or MAP2 and Tuj1 double stain (see Supplementary Figs. 2A–B").

Cajal-Retzius cells play an important role in the normal layer formation of the hippocampus. The Tbr1/reelin double staining revealed that Cajal-Retzius cells (Nakajima et al., 1997), some of which were Tbr1-positive, were present in the mutant (Fig. 2P). The hippocampal fissure, which is characterized by Reelin-positive cells, was poorly developed (asterisk in Figs. 2O and P). In the developing p73⁻/⁻ hippocampus, the most striking abnormality is the absence of the hippocampal fissure, which suggests a role for p73 in cortical folding (Meyer et al., 2004). Therefore, p73 and Reelin expression were examined at the cortical hem (see Supplementary Fig. 4), which revealed that the expression of p73 and reelin was both normal in *RP58*-deficient cortical hem. We next examined the CA and DG. The

pan-hippocampal plate marker, α-crystalline (Funatsu et al., 2004), was expressed in a more dorsal cortical region in the mutant than in the wild type (arrows in Figs. 4A and E). Since α-crystalline is also expressed in the neocortex as well as in the hippocampus, we used another hippocampal marker, α-synuclein, together with the DG marker, Prox1. We found that α-synuclein was expressed in the hippocampal region and its staining did not overlap with the Prox1-positive region in the wild-type brain. In contrast, although α-synuclein expression was detected in the more dorsal cortical region in the mutant brain, it did not overlap with the Prox1-positive dentate region (see Supplementary Figs. 5A–B"). These results suggested that the hippocampus was formed in a more dorsal region in the mutant, probably because of an insufficiency in hippocampal folding; however, the basic positional relationship between the CA and DG remained intact.

Furthermore, we examined whether specific hippocampal subfields were generated in the *RP58*-deficient mice. The expression of the CA3-specific marker KA1 (Grik4) (Bettler et al., 1990) was almost undetectable (an arrow in Figs. 4B and F). The CA1-specific marker SCIP (Pou3f1) (Frantz et al., 1994; arrows in Fig. 3C) was not detected (Fig. 4G). NT3, which is expressed in the cingulate neopallium (Friedman et al., 1991; Lee et al., 2000; an arrow in Fig. 4D), was also not detected in the mutant (Fig. 4H). To examine the DG, we used Prox1 and NeuroD (Figs. 2Q–T), which are markers of immature dentate granule cells (Pleasure et al., 2000; Galichet et al., 2008). In the wild type, Prox1- and NeuroD-positive cells formed a V-shaped structure, which is typical of the DG, whereas in the mutant they formed an inverted V-shaped structure (arrowhead in Figs. 2Q–T). The DG region that was positive for Prox1 appeared to extend throughout the *RP58* mutant hippocampus (Supplementary Fig. 6), suggesting that loss of RP58 function may result in an increase in the number of Prox1-positive dentate granule cells. It is reported that Tbr1 is expressed after onset of NeuroD expression (Hevner et al., 2006). Tbr1 was expressed in many NeuroD-positive dentate granule cells in the wild type, whereas its expression was severely reduced in the mutant (Figs. 2S and T), suggesting that the production of mature neurons is impaired in the mutant dentate granule cells. These results suggest that, although major areas of the hippocampus were probably retained in the mutant, the CA1, CA3 fields, the cingulate cortex, and DG were not, indicating that the hippocampal neurons had maturation defects like those seen in the neocortex.

Expression pattern of RP58 protein

The abnormality of neurons generated in the mutant cortex indicates that RP58 functions during the development of the neocortex

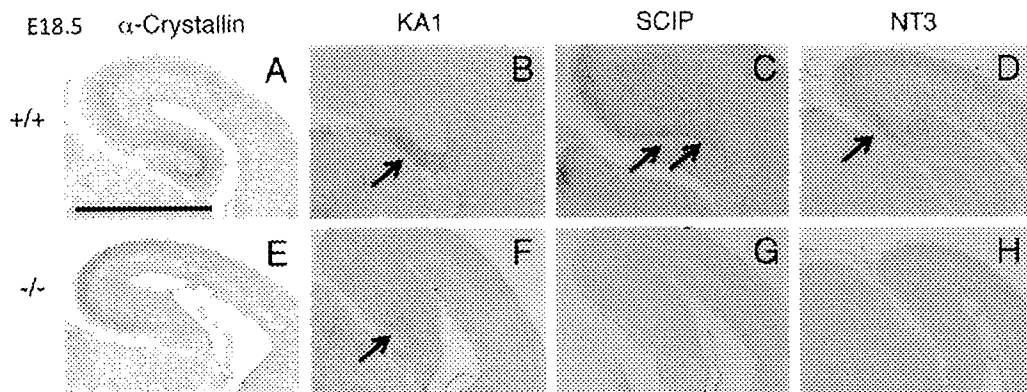E18.5   α-Crystallin   KA1   SCIP   NT3

+/+

-/-

Fig. 4. Field specification impairment in the hippocampus of *RP58*-deficient E18.5 mice. α-crystalline, which is a pan-hippocampal marker, was detected in the hippocampal region of the wild-type brain (arrows in A), whereas it was detected in the more dorsal region in the *RP58*-deficient brain (arrows in E). The expression of the CA3-specific marker KA1 (an arrow in B) was almost not detected in the mutant brain (an arrow in F). In the wild-type brain, SCIP was expressed in CA1 sector of the hippocampus (arrows in C) and in the adjacent cortex, while it was not detected in the mutant brain (G). NT3, which is a cingulate neopallium marker (an arrow in D), was not detected in the mutant (H). Scale bar, 1 mm (A–H).

and of the hippocampus. To further understand the function of RP58, we examined the expression patterns of the RP58 protein using an RP58-specifc antibody (Takahashi et al., 2008). The immunostaining pattern obtained was almost identical to that of the RP58 mRNA *in situ* hybridization pattern (Figs. 5A and B). The specificity of the RP58 antibody was confirmed by immunostaining of an *RP58⁻/⁻* brain (Fig. 5C). Double staining using the nuclear marker TOPR3 showed that RP58 was localized in the nucleus and that it was absent from the cytoplasm (Supplementary Figs. 7B and 8''). At E12.5, RP58 was detected in preplate neurons and in some cells in the VZ (arrows in Fig. 5D). At E16.5, RP58 was present in the CP, IZ, SVZ, and in some cells in the VZ (arrows in Figs. 5E and E'), but not in cells of the MZ (Fig. 5E). Double staining with β-synuclein or Reelin indicated that RP58 was expressed in subplate neurons (arrows in Fig. 5F), but not in Cajal-Retzius cells (Fig. 5G; Supplementary Fig. 8). RP58 was not detected in Dlx2-positive cells (arrows in Fig. 5I), which correspond to GABAergic neurons. In the E16.5 hippocampus. RP58 was detected in most developing neurons and in some progenitor cells in the VZ (Fig. 5J). At E18.5, RP58 was detected in migrating neurons, pyramidal layer cells of the CA, and dentate granule cells (Fig. 5K), which were identified by immunoreactivity for NeuroD (Figs. 5L and L'). RP58 was not detected in reelin-positive Cajal-Retzius cells in the hippocampal fissure (asterisk in Fig. 5K). Therefore, RP58 is expressed in migrating and

postmigratory glutamatergic neurons, which are impaired in the mutant, whereas RP58 is not expressed in the Cajal-Retzius cells and GABAergic neurons, which are not impaired in RP58-deficient animals. as shown in Fig. 2. Interestingly, RP58 is also expressed in the progenitor cells in the VZ. Interestingly, some cells in the VZ expressed the RP58 protein at a high level (arrows in Fig. 5H; Supplementary Figs. 7A–8''), and other cells expressed this protein at a low level (arrowheads in Supplementary Figs. 7A–8''). As all of these cells were positive for Ki67, a nuclear protein expressed only in cycling cells. this result suggests that RP58 is expressed by neural progenitors.

To examine whether the VZ cells that express RP58 are RGPs and/or IMPs, we performed double labeling of RP58 with Pax6 (which is an RGP marker) and Tbr2 (which is a pan-IMP marker). Most of the RP58-positive cells in the VZ were Tbr2-positive (arrows in Supplementary Figs. 9C–C'''), whereas some RP58-positive cells were Pax6-positive (arrows in Supplementary Figs. 9A–B''') and the others were Pax6-negative (arrowhead in Supplementary Figs. 9A–B'''). RP58 was expressed in P-H3-positive cells in the basal regions of the VZ, but not in the apical region of the VZ (Supplementary Fig. 10). RP58 was also detected in some of Ngn2-positive cells (Supplementary Fig. 11). These results suggest that the onset of RP58 expression happens during the transition from Pax6-positive cells to Tbr2-positive cells, or, in other words, at the initial stage of IMPs.
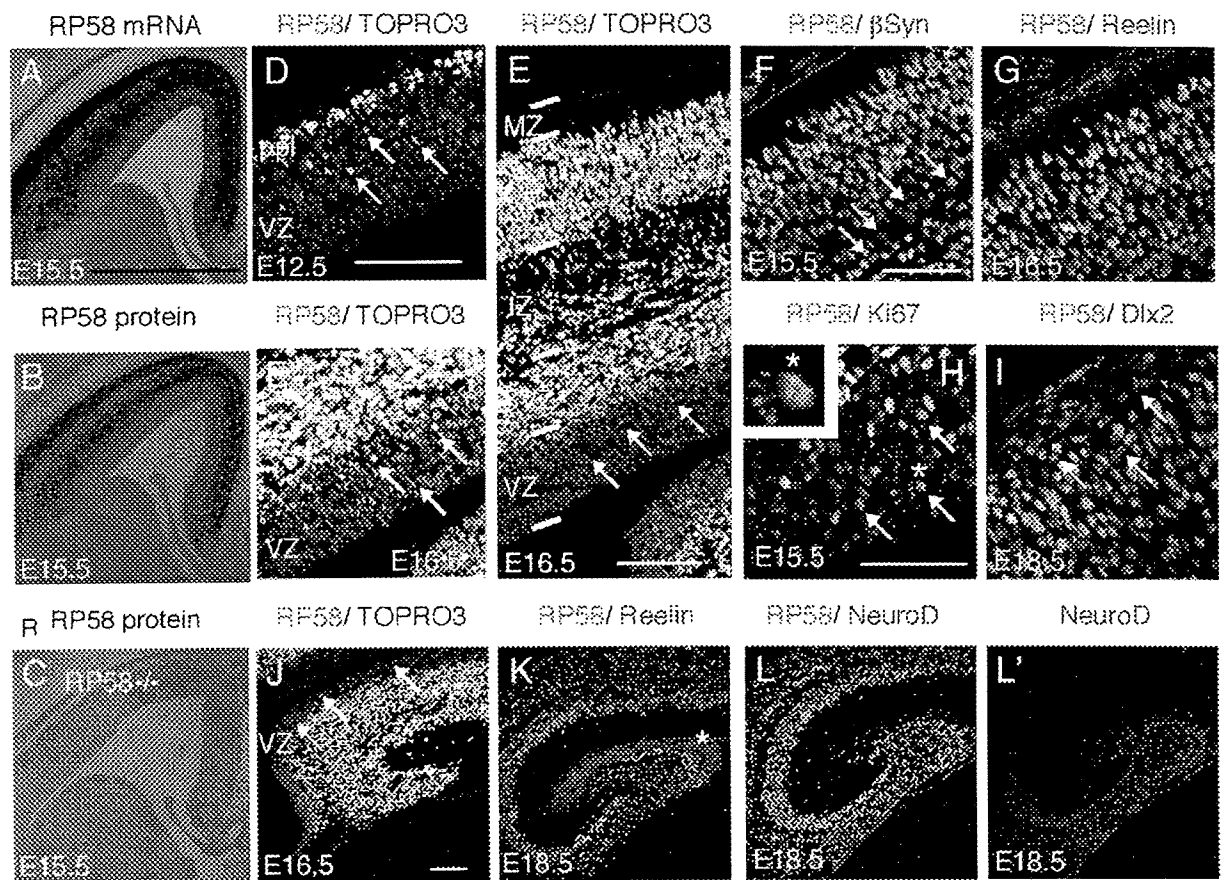

Fig. 5. RP58 expression patterns in the wild-type cerebral cortex. (A) RNA *in situ* hybridization analysis shows that RP58 transcripts were strongly expressed in cortical cells in the CP, IZ, SVZ, and weakly in the VZ of E15.5 wild-type mice. (B and C) RP58 protein was detected at high levels in the CP, IZ, and SVZ, and weakly in the VZ of E15.5 wild-type mice (B). No signal was detected in RP58⁻/⁻ brain (C). (D, E, and E') RP58 protein was intensely expressed in developing neurons in the preplate (ppl) at E12.5 (D), in the CP, IZ, and SVZ at E16.5 (E), and in progenitor cells in the VZ at E12.5 (arrows in D) and E16.5 (arrows in E and E'). (F–I) RP58 was detected in β-synuclein-positive subplate neurons at E15.5 (F) and was not detected in the reelin-positive Cajal-Retzius cells at E16.5 (G). Ki67, which is a cell cycling marker. was detected in RP58-positive cells in the VZ at E15.5 (H). A higher magnification view of the region marked by an arrow with an asterisk (*) indicates that RP58 protein was expressed in Ki67-positive progenitor cells. RP58 was not detected in Dlx2-positive GABAergic neurons in the E18.5 neocortex (I). (J) RP58 was expressed in progenitors cells in the VZ (arrows in J) and in the developing neurons of the E16.5 hippocampus. (K–L') RP58 was not detected in reelin-positive Cajal-Retzius cells in the hippocampal fissure (asterisk. K) at E18.5. RP58 was detected in NeuroD-positive DG granule cells (L, L') at E18.5. Scale bars, 1 mm (A–C); 0.1 mm (D and E'), (E), and (J–L'); and 0.05 mm (F, G and I). (H).

Enhanced apoptosis in the RP58-deficient cortex

Next, we examined whether enhanced cell death or reduced production of cortical neurons in the mutant cortex were responsible for the fewer numbers of mature subplate and specified CP neurons observed in the mutant cortex. A larger number of TUNEL-positive cells were found in the postmitotic zone of the mutant neocortex at E15.5 and E18.5 when compared with the wild type, but no differences were observed in the proliferative zone (Figs. 6A, B, E, and F; Supplementary Fig. 12). The mutant hippocampus displayed a significant increase in the number of TUNEL-positive cells at E18.5 when compared with the wild type (Figs 6M and N). Active-caspase3 immunoreactivity was also enhanced at E16.5 (Figs. 6C, D, I, and J) and E19 (Figs. 6G, H, O, and P) in both the neocortex and the hippocampus of the mutant mice, which suggests that caspase-dependent apoptosis is enhanced in the mutant. Apoptosis was detected in the anterior and posterior neocortex to the same degree (data not shown). Furthermore, single-strand DNA (ssDNA) staining using an anti-ssDNA antibody documented the presence of fragmented DNA (Figs. 6K and L), which confirmed the results of the TUNEL analysis. These results suggest that RP58 deficiency enhances caspase-dependent apoptosis in the cerebral cortex, which may reduce the number of mature cortical neurons.

Expansion of the VZ/SVZ in the RP58-deficient cortex

In addition to enhanced apoptosis, we found that the VZ was likely to be expanded in the postnatal day (P) 0 mutant cortex (asterisk in Fig. 1B). We therefore examined the expression of several markers of the VZ, which included Pax6 (Englund et al., 2005). Pax6 expression expanded radially in the mutant cortex at E19 when compared with the distribution of this protein in the wild-type cortex at E19, as did PCNA immunoreactivity (Figs. 7A–B″). Furthermore, the expression of HES5, which is a basic helix–loop–helix transcription repressor expressed in the VZ (Ohtsuka et al., 2006), and of Tailless, which is an orphan nuclear receptor restricted to the VZ (Monaghan et al., 1995), was also enhanced in the mutant neocortex (Figs. 7C–F). The VZ was expanded in the hippocampus as well as in the neocortex, as determined by double staining of Pax6 with PCNA or Ki67 at E18.5 (Supplementary Fig. 13).

Next, we examined whether IMPs were increased in the mutant. Tbr2-positive cells, which are detected in IMPs and postmitotic immature neurons (Englund et al., 2005), were increased in the E18.5 mutant (Supplementary Figs. 14A and B). The phosphohistone H3 (P-H3)-positive mitotic cells in the SVZ, which correspond to mitotic cells of IMPs, were also increased, together with PCNA-positive cells (see Supplementary Figs. 14C–D′). These results suggest that IMPs were
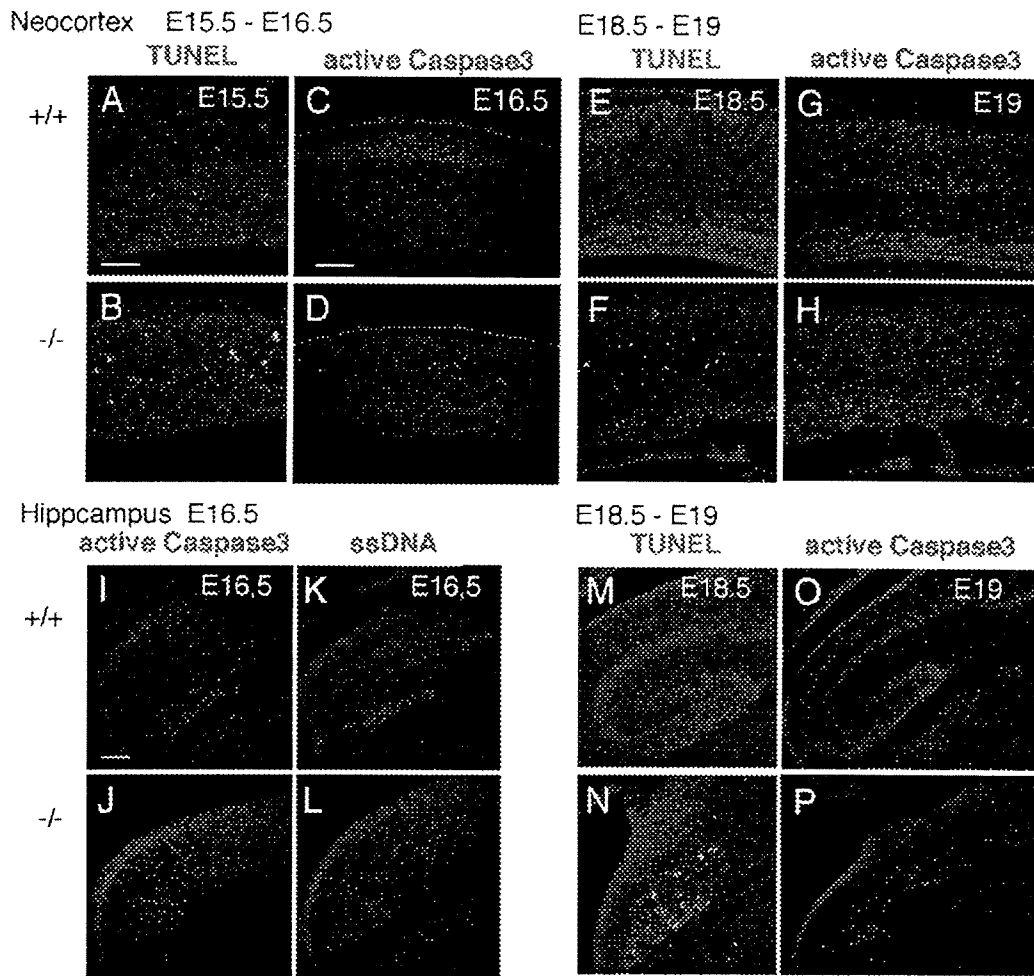

Fig. 6. Enhancement of apoptosis in the RP58-deficient cortex. (A–H) In the mutant neocortex, the number of TUNEL-positive cells was higher than in wild type at E15.5 (A and B) and E18.5 (E and F), and the number of active-caspase 3-positive cells was higher at E16.5 (C and D) and E19 (G and H). (I–P) In the mutant hippocampus, active-caspase 3-positive cells (I and J) and ssDNA-positive cells (K and L) were increased at E16.5 and TUNEL-positive cells and active-caspase 3-positive cells were also increased at E18.5 (M–P). Scale bars, 0.1 mm (A, B, E, F, M, and N), (C, D, G, H, O and P), and (I–L).
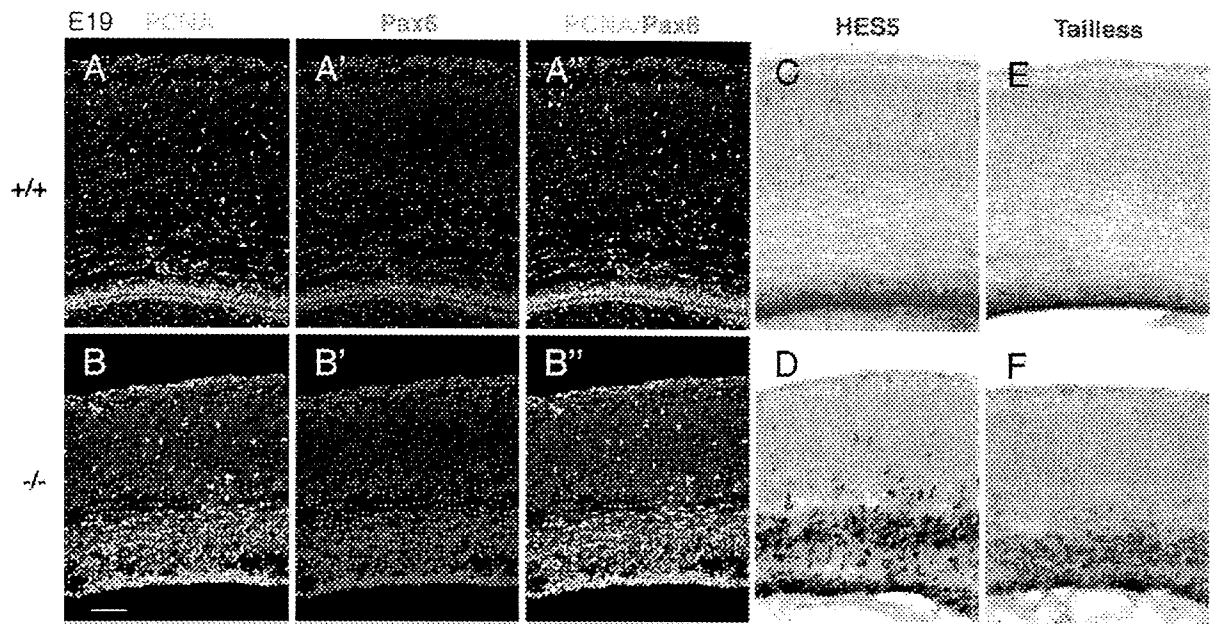
Fig. 7. Expansion of the ventricular zone in the RP58-deficient cortex. (A–B″) PCNA-positive cells and Pax6-positive cells were increased in the RP58⁻⁻ cortex (A–B′) and most Pax6-positive cells were immunoreactive for PCNA (A″ and B″). (C–F) The RP58⁻⁻ cortex (D and F) exhibited more HES5-positive cells (C and D) and Tailless-positive cells (E and F) than the wild-type cortex (C and E). Scale bar, 0.1 mm (A–F).

increased in the mutant. To examine the developmental stage of IMPs, we performed double staining of Tbr2 and Pax6 (Fig. 8), as Pax6+/Tbr2+ cells and Pax6−/Tbr2+ cells are early-stage IMPs and late-stage IMPs, respectively (Sasaki et al., 2008). The double staining revealed that, in the E18.5 mutant, Tbr2-positive cells and Pax6-positive cells were increased in number, that both Pax6+/Tbr2− cells and Pax6+/Tbr2+ cells were also increased, whereas Pax6−/Tbr2+ cells were not (Fig. 8). This result suggests that RGPs and early-stage IMPs were increased in the mutant, whereas late-stage IMPs were not. To examine the identify of the SVZ, we preformed Svet1 in situ hybridization near the section of the Pax6/Tbr2 double staining from E15.5 to E18.5, which revealed that impairment of the mutant VZ/SVZ progressed from E15.5 to E18.5 (Supplementary Fig. 15). In particular, a tripartite appearance of inner Pax6-dominant/intermediate Tbr2-dominant/outer Pax6-dominant zones was observed in the mutant in later developmental stages (Supplementary Fig. 15). To directly associate these zones with Svet1 expression, we performed a triple staining of Pax6, Tbr2, and Unc5d that corresponds to Svet1 (Sasaki et al., 2008) (Supplementary Fig. 16). Unc5d/Svet1 staining was detected in the upper region of the Tbr2-positive zone in the wild type, while it was also detected, albeit weakly and diffusely, in the upper region of the intermediate Tbr2-positive zone and contained the outer Pax6-dominant zones in the E16.5 mutant mice (Supplementary Figs. 16 A–B′), which suggests that the outer Pax6-dominant zone was located in the SVZ. In the E18.5 mutant, the expression of Unc5d/Svet1 was more diffusely detected in the outer Pax6-dominant/intermediate Tbr2-dominant zone, which suggests that the mutant VZ/SVZ was severely impaired in the late development stages of the mutant (Supplementary Figs. 16 C–D′).

The impairment of cell-cycle exit in the RP58-deficient VZ/SVZ during late development

We next examined whether the expansion of the VZ/SVZ of the mutant cortex was due to enhanced proliferation and/or impairment of cell-cycle exit. To examine cell proliferation, we counted the number of BrdU-labeled cells in a random selection of 50 Ki67 (which is a proliferating cell marker)-positive cells (which are considered to

be progenitor cells) after a 30 min pulse of BrdU. The percentage of progenitor cells labeled with BrdU was not altered in the mutant cortex at E15.5, which suggests that proliferation was not altered in the mutant cortex (Figs. 9A–C). To examine the possibility that the division pattern of progenitor cells was impaired in the mutant cortex, we counted the number of PCNA-negative and Pax6-negative cells in a random selection of 50 BrdU-labeled cells, after a 24 h pulse of BrdU; this corresponds to the fraction of cells exiting the cell cycle. At E16.5, we found that the PCNA−/BrdU+ and Pax6−/BrdU+ ratios were about halved in RP58 mutant progenitor cells when compared with their normal counterparts, which suggests that cell-cycle exit is inhibited in the mutant VZ progenitor cells in both the medial and lateral neocortices (Figs. 9D–I). This was confirmed by examining the total number of BrdU-positive cells in an area of 0.25 mm², which showed an increase in the number of PCNA− or Pax6+ cells; this suggests that reentry into the cell cycle is enhanced in the mutants (Supplementary Fig. 17). Furthermore, as the characteristic outer Pax6-dominant zone was observed in the mutant cortex (Supplementary Fig. 16B), we examined whether the outer Pax6-dominant zone was involved in the reduction of cell-cycle exit. The Pax6−/BrdU+ ratio was dominantly reduced in the upper region (IZ/SVZ), which contained the abnormal outer Pax6-dominant, when compared with the lower region (VZ) (Supplementary Fig. 18). Therefore, it is possible that the abnormal outer Pax6-dominant zone observed in the mutant reflects the reduction of cell-cycle exit. In contrast, neither proliferation at E12.5 (Supplementary Figs. 19A–C) nor cell-cycle exit at E13.5 (Supplementary Figs. 19D–I) was impaired. These results suggest that cell-cycle exit is reduced in the mutant cortex at late neocorticogenesis. The reduction of the cell-cycle exit causes an increase in VZ progenitor cells and thereby leads to the expansion of the VZ. Therefore, it is likely that the reduction of cell-cycle exit, in addition to the enhanced apoptosis, decreases the number of differentiated late-born neurons in the mutant CP.

As cell-cycle kinetics may affect cell-cycle exit, we estimated the duration of the S-phase (Ts) and of the total cell-cycle time (Tc) using a BrdU/IdU double labeling paradigm (Martynoga et al., 2005), which revealed no obvious differences in Ts, Tc, and Ts/Tc between wild-type and mutant cortices (Supplementary Fig. 20); however, because this
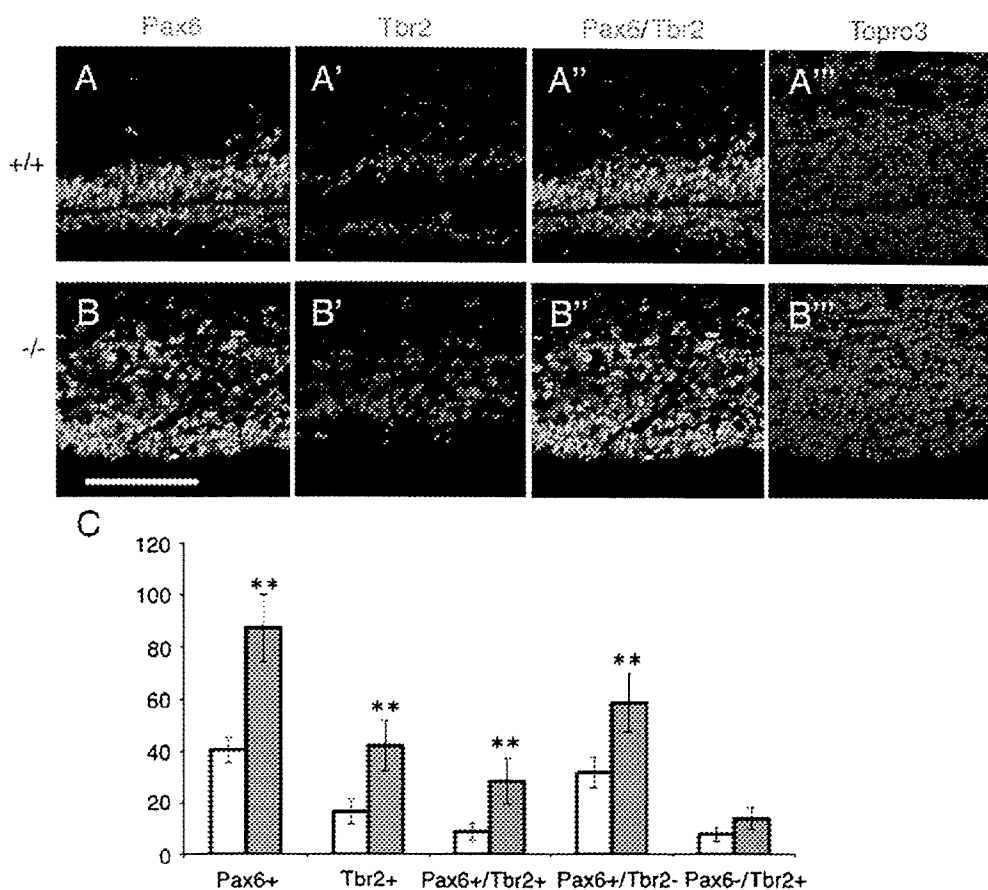
Fig. 8. Both Pax6-positive and Tbr2-positive cells were increased in the RP58-deficient cortex. Double staining (A", B") of Pax6 (A, B) and Tbr2 (A', B') with the TOPRO3 nuclear stain (A''', B''') showed that both Pax6-positive and Tbr2-positive cells were increased in the RP58-deficient cortex. Scale bars, 0.1 mm (A–B'''). (C) The number of Pax6 +, Tbr2 +, Pax6 +/Tbr2 +, Pax6 +/Tbr2 -, Pax6 -/Tbr2 -, and Pax6 -/Tbr2 + cells was counted in a 0.0083 mm² area of the wild-type (open column) and of the mutant neocortex (gray column). Faint staining of Pax6 was regarded as negative. Six regions of three mutant brains were compared with six regions of three wild-type brains. The data are presented as means ± SD. **P < 0.01 (Student's t test).

estimation rested on the assumption that all cells in the VZ are proliferating and that the precursor cells consist of a single proliferating population with the same cycling kinetics (Martynoga et al., 2005), further analyses may be necessary to assess the possibility that RP58 is involved in cell-cycle kinetics.

Discussion

In the present study, we characterized mice carrying disrupted alleles for the POZ/zinc finger transcriptional repressor gene, RP58. We found that homozygous mutants display severe hypoplasia of the cerebral cortex and of the hippocampus, in association with enhanced apoptosis and expansion of the VZ/SVZ. We showed that RP58 is specifically required for the maturation and survival of the excitatory neurons of the cerebral cortex. Furthermore, the present study demonstrated that RP58 is a novel factor that controls the balance of cell division of neuronal progenitors, which remains poorly understood to date.

In the RP58 null mutant, the VZ was expanded and the dorsal cortex appeared like a wild-type younger brain. Therefore, the possibility of developmental delay cannot be excluded. We examined the expression of Tbr1 in the mutant cortex at E13.5, E15.5, and E18.5, which suggested that there is no clear time lag in the Tbr1 expression pattern (Supplementary Fig. 3). In addition, the Tc may cause a developmental delay. The Tc was not altered in the RP58-deficient mice (Supplementary Fig. 20). These results do not support the contention that developmental delay mainly occurs in RP58 null mice.

It seems more likely that reduction of produced matured neurons and enhancement of apoptosis causes the impairment in cortical development observed in these animals.

One of the main phenotypes in the RP58-deficient cortex was a reduction in the number of mature cortical neurons. In addition to a substantial reduction in the number of neurons in the subplate and layers 2–5 of the CP in the neocortex, Tbr1 expression was strongly suppressed throughout the cortical anlage, with the exception of the Cajal-Retzius cells in the hippocampus. The pyramidal layer of the CA was absent and Tbr1 expression was severely reduced in NeuroD-positive granule cells of the DG. NeuroD is expressed after Pax6, but before Tbr1 (Hevner et al., 2006), which suggests that RP58 deficiency suppresses the production of mature dentate granule neurons.

In the early embryonic stage, RP58 deficiency did not impair cell-cycle exit, although apoptosis was enhanced in the mutant neocortex at E15. Therefore, the decreased number of mature subplate neurons produced at early embryonic stages could be caused by enhanced apoptosis. On the other hand, the VZ was expanded at later embryonic stages in the mutant, the cell-cycle exit was inhibited in RGPs, and the level of apoptosis remained high, which suggest that enhanced apoptosis and/or defective cell-cycle control reduce the production of mature cortical neurons at later development stages.

Transgenic mice expressing β-catenin precursors also show reduced cell-cycle exit and develop enlarged brains with reduced cortical thickness (Chenn and Walsh, 2002). In contrast, RP58⁻/⁻ mice showed no enlargement of the brain, although the thickness of the neocortex was reduced. This discrepancy may be due to the reduction

E15.5 (BrdU 0.5hr)
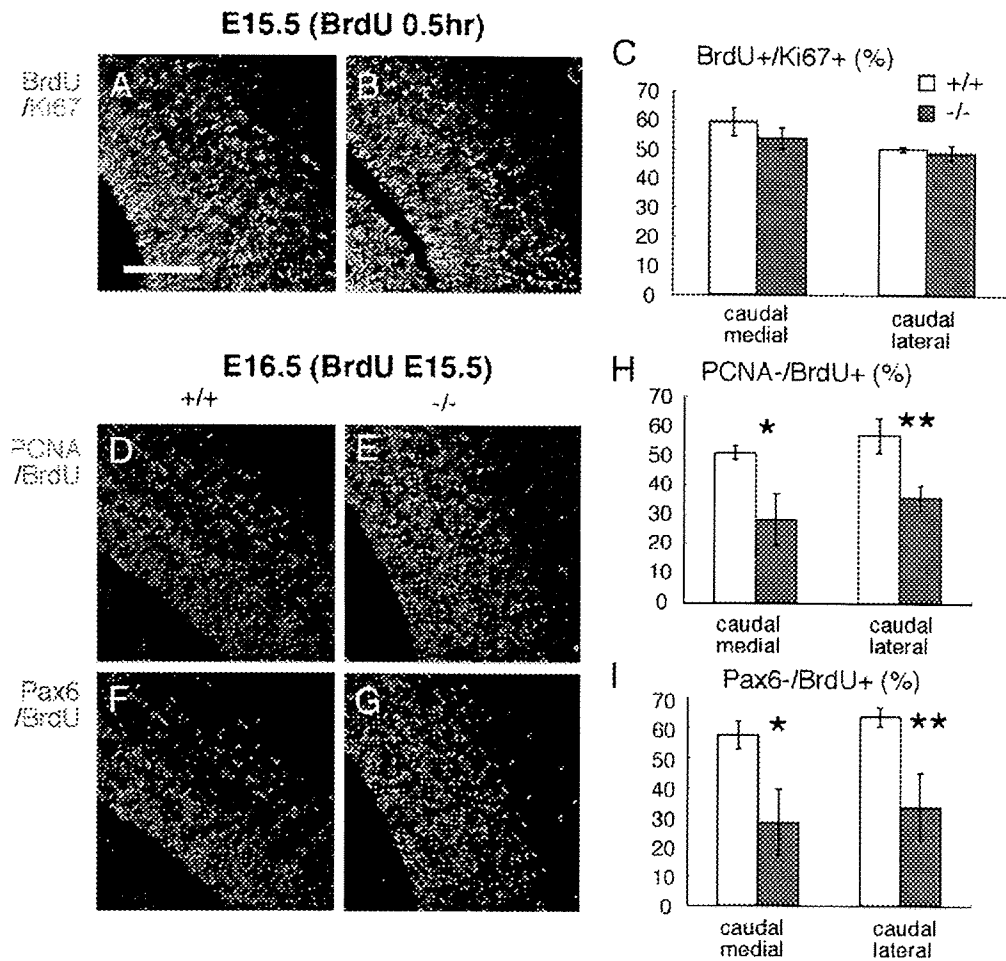

E16.5 (BrdU E15.5)

Fig. 9. Impairment of cell-cycle exit in the *RP58*-deficient cortex in late neocortical development. (A–C) Double labeling with BrdU and Ki67 in the lateral region of the wild-type (A) and mutant (B) caudal neocortex at E15.5, 0.5 h after BrdU incorporation. The fraction of BrdU-positive cells among the Ki67-positive cells was not altered in the medial and lateral regions of the mutant cortex (C), which suggests that proliferation is not affected in the mutant cortex. Fifty Ki67-positive cells were randomly examined. Four regions of two mutant brains were compared with six regions of three wild-type brains. (D–I) BrdU was incorporated at E15.5 and the lateral region of the caudal neocortex was double stained for BrdU and PCNA (D and E) or Pax6 (F and G) in the lateral region of the wild-type (D and F) and the mutant (E and G) at E16.5. The fraction of PCNA-negative cells and Pax6-negative cells among the BrdU-positive cells was reduced in the caudal *RP58*-deficient cortex in both the medial and lateral regions of the mutant caudal neocortex (H and I), which suggests that cell-cycle exit was reduced. Fifty BrdU-positive cells were randomly examined. Three regions of three mutant brains were compared with three regions of three wild-type brains. Scale bar, 0.1 mm (A–D, G, and H). The data are presented as means ± SD. *$P < 0.02$, **$P < 0.01$ (Student's t test).

of cell-cycle exit only at late embryonic stages and/or the presence of high levels of apoptosis in the RP58$^{-/-}$ cortex. We consider RP58 a candidate molecule for the control of the number of mature cortical neurons, as RP58 deficiency decreased the number of mature neurons because of enhanced apoptosis and of defects in cell-cycle exit.

A delicate balance in cell proliferation and subsequent cell-cycle withdrawal and differentiation into specific neurons is essential for corticogenesis. The present study indicates the possibility that RP58 regulates this balance, at least at the late embryonic stage. In the wild-type E15.5 VZ, some RP58-positive cells showed weak Pax6 immunoreactivity, and almost all RP58-positive cells exhibited Tbr2 immunoreactivity (Supplementary Fig. 9), which suggests that the onset of RP58 expression happens in IMPs, at the initial stage, when Pax6 and Tbr2 may be coexpressed (Englund et al., 2005).

Pax6+ cells were increased in the RP58 null mutant, as were both Pax6+/Tbr2− and Pax6+/Tbr2+ cells. The increase in the number of Pax6+/Tbr2− cells in the mutant is explained by the reduction of cell-cycle exit of VZ progenitors. It is likely that there are extrinsic actions that allow RP58 to activate the expression of extrinsic factors that control cell-cycle exit, because RP58 is not detected in most Pax6+ cells. In fact, it is reported that the generation of projection

neurons from cortical progenitors appears to be governed by both cell-intrinsic and environmental cues (Mizutani and Gaiano, 2006); however, we cannot exclude the possibility that a few Pax6+ cells abnormally proliferated in the mutant, as RP58 was detected in some Pax6+ cells in the wild type.

Pax6+/Tbr2− and Pax6+/Tbr2+ cells were increased in the mutant VZ/SVZ, whereas Pax6−/Tbr2+ cells were not increased. Therefore, it is possible that Pax6 is ectopically expressed in Tbr2+ IMPs in the mutant, and that the transition from Pax6+/Tbr2+ cells to Pax6−/Tbr2+ cells was inhibited in the mutant, which raises the possibility that RP58 may be an important molecule for the maturation of IMPs. It was reported that (1) Svet1 is a spliced intronic sequence from Unc5d (Sasaki et al., 2008) and (2) Svet1/Unc5d staining is a specific marker of late-stage IMPs. It is likely that Svet1/Unc5d expression was reduced in the mutant, which supports the possibility that RP58 is most important for maturation process from early-stage IMPs to late-stage IMPs; however, as the expression of Svet1/Unc5d is also observed in young neurons (Kawaguchi et al., 2008), the possibility that the reduction of Svet1/Unc5d signal in the mutant reflects the reduction of the number of generated neurons cannot be excluded.